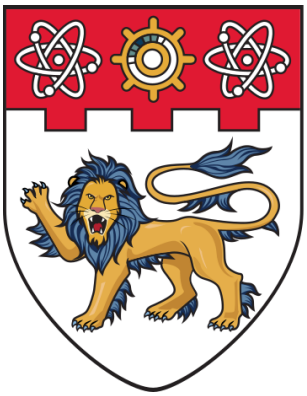

NANYANG TECHNOLOGICAL UNIVERSITY

SINGAPORE

ANALYSIS OF DEFORMATION OF SETAE ON THE FIRST ANTENNAE OF COPEPODS

RAPHAEL LEE JIA YING

G1802350L

SCHOOL OF MECHANICAL AND AEROSPACE ENGINEERING

2023

ANALYSIS OF DEFORMATION OF SETAE ON THE FIRST ANTENNAE OF COPEPODS

RAPHAEL LEE JIA YING

SCHOOL OF MECHANICAL AND AEROSPACE ENGINEERING

A thesis submitted to the Nanyang Technological University in partial fulfilment of the requirement for the degree of Master of Engineering

2023

Statement of Originality

I hereby certify that the work embodied in this thesis is the result of original research, is free of plagiarised materials, and has not been submitted for a higher degree to any other University or Institution.

[12 December 2022]

. . . . . .

Date

. . . . . .

[Raphael Lee Jia Ying]

Supervisor Declaration Statement

I have reviewed the content and presentation style of this thesis and declare it is free of plagiarism and of sufficient grammatical clarity to be examined. To the best of my knowledge, the research and writing are those of the candidate except as acknowledged in the Author Attribution Statement. I confirm that the investigations were conducted in accord with the ethics policies and integrity standards of Nanyang Technological University and that the research data are presented honestly and without prejudice.

[12 December 2022]

. . . . . .

Date

. . . . . .

[A/P Marcos]

Authorship Attribution Statement

This thesis **does not** contain any materials from papers published in peer-reviewed journals or from papers accepted at conferences in which I am listed as an author.

[12 December 2022]

. . . . . .

Date

. . . . . .

[Raphael Lee Jia Ying]

Acknowledgements

First and foremost, I would like to extend my greatest gratitude to my supervisor, Associate Professor Marcos from Nanyang Technological University for making this work possible. His guidance and advice carried me through all the stages of this study. Associate Professor Marcos has constantly monitored my progress and motivated me in the correct direction of work.

I would also like to give special thanks to my second mentor, Dr. Shen Xinhui, whom has also generously shared his ideas, guided me with the respective methods and patiently explaining to me the correct concepts to apply for this study.

This work would not have been possible without the help from Associate Professor Marcos and Dr. Shen Xinhui for their vast experience in research. The unwavering support from both my mentors have significantly contributed in the possibility of this study. I am sincerely grateful to them for the amount of time and effort put in to nurture my research and writing skills over the course of my study in the M. Eng programme.

Abstract

Copepods are small crustaceans that rely on their mechanoreceptors which are biologically linked to setae present on the first antennae of copepods to carry out daily activities such as predating and escaping from prey. Mechanoreceptors of copepods detect hydrodynamic disturbances induced by other organisms in the surroundings by bending of setae on the first antennae which triggers a neural signal to elicit a reaction. The process of detection is very efficient and most of the studies on mechanoreception focus only on the relationship between a copepod's physiological and behavioural responses, but lacking in the physical threshold aspect.

This experimental study aims to investigate the stiffness of setae by studying the physical threshold of setal deformation when subjected to hydrodynamic disturbance in the form of artificial stimulus. The current work using *Pseudiaptomus annadalei* as the specimen has shown significant experimental results for this study's progress. Morphological observations are similar to past studies, finding two types setae present on the first antennae, smooth and long, as well as short and tapered. The first antenna's length measures at 1040 µm approximately and the smooth and long type of seta has an average length of 84 µm. To produce artificial stimulus, a syringe pump is used in conjunction with a tubing line which connects to a syringe tip that is submerged in the same medium as the specimen. The syringe then injects water through the tubing line to the syringe tip outlet which creates hydrodynamic disturbance in the same medium as the copepod. This hydrodynamic force is subjected onto setae on the first antenna perpendicularly, to achieve setal deformation in both directions, towards the distal tip of the antenna and proximally towards the body are observed.

The purpose of the siphon flow device is to fix the outlet position which is connected to the syringe pump to better define the artificial stimulus and setal deformation. This device is able to produce a constant and quantifiable flow as the artificial stimulus as compared to past studies, in order to attain more accurate measurements of setal deformation. These experiments will then be translated to quantify the deformation of setae on the first antenna, based on the flow velocity that each seta is subjected to. A simple spring model which depicts the resistance at the setal root utilizes the flow velocities, deformation and morphological results, based on the Resistive Force Theory, to estimate the spring constant of the long and smooth type of seta.

Contents

List of Figures

List of Symbols

u	The fluid velocity
u_r	The radial velocity component of the fluid
u_θ	The tangential velocity component of the fluid
A	The first constant that depends on the geometry and rotational speed of the two cylinders
B	The second constant that depends on the geometry and rotational speed of the two cylinders
r	The distance from the centre to a point within the annular space
μ	The dynamic viscosity of the fluid
ρ	The density of the fluid
p	The pressure of the fluid
ω	The angular velocity of the inner cylinder
R_i	The radius of the inner cylinder
R_o	The radius of the outer cylinder
Hz	The number of cycles in one second
v	The flow velocity of the fluid in the medium

1 Introduction

1.1 Background of Copepods

Copepods are a group of small crustaceans that live in most freshwater and saltwater habitats. A typical copepod can grow up to 1 to 2 millimetres across various species and are known for a teardrop shaped body with long antennae as seen in Figure 1-1 (a). Figure 1-1 (b) shows the positions of the copepod appendages relative to the copepod body. The first antennae are attached at the top of its head which contains sensory structures [1] to detect nearby prey and predators [2]. The feeding appendages beat in the frequency ranging from 20 Hz to 80 Hz [3] to form a feeding current to pull the prey towards its mouthpart. The swimming appendages kick sequentially for copepods to move around the habitat and escape from predators.

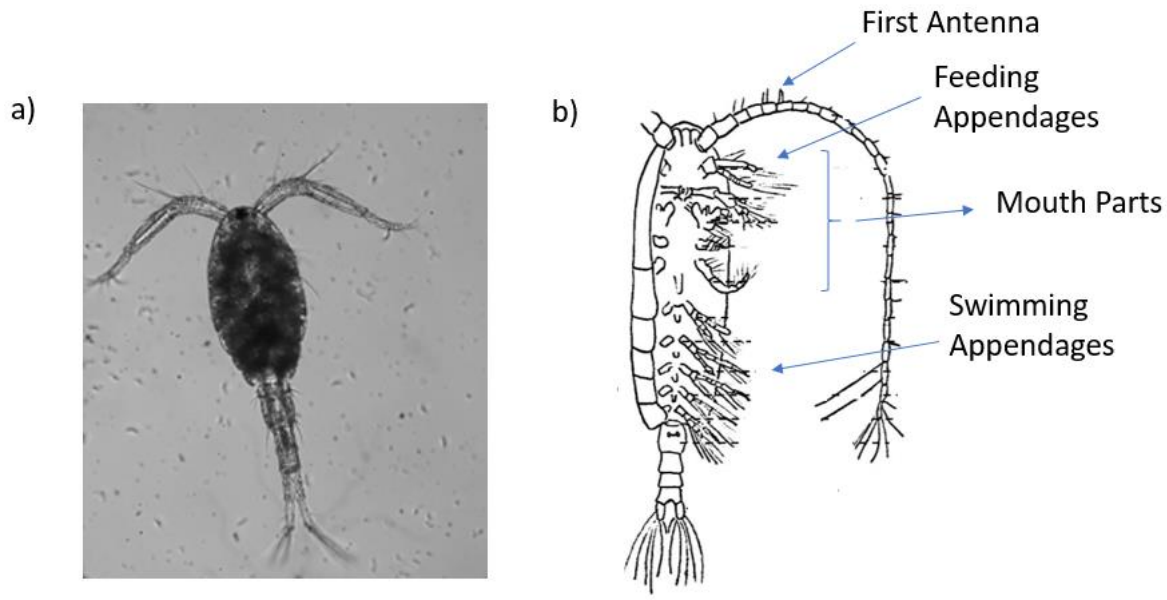

Figure 1-1 a) Image of Tigriopus californicus viewed under a microscope b) Schematic drawing of a calanoid copepod's external morphology, showing its first antenna, feeding appendages, mouth parts and swimming appendages. Adopted from Koehl et al. [4]

Copepods grow in several stages with gradual development of their features and body size. Their life cycle in made up of 14 stages, as shown in Figure 1-2 [5], with the main phases

starting from an egg that hatches to a nauplii, growing into a copepodite and finally an adult. A nauplii is characterized by head and tail segments without significant thorax or abdomen. As the nauplii develops into a copepodite, some of its swimming and feeding appendages grow along with its first antennae. Moreover, a copepodite moults several times before it reaches the adult stage. At the adult stage, the copepod's first antennae are fully grown, with an additional pair of both feeding and swimming appendages which are lacking in the copepodite stage. A full development process of copepods can range from a week to a year depending on the species, and they can live up to six months to a year.

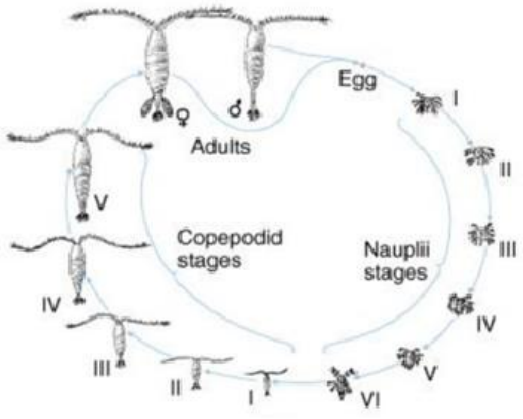

Figure 1-2 Copepod Life Cycle. Adopted from Koehl et al. [4]

1.2 Sensory Structures of Copepods

Copepod reacts with the environmental cues through the sensors known as setae. The copepod setae are hair-like structures [6] that protruding from the first antennae and other appendages. Setae are classified into two types in terms of their functionalities, chemoreceptional and mechanoceptional [7]. The former senses pheromone trials or plumes left behind by the female [8], while the latter responds to hydrodynamic disturbances created by prey or predators nearby [9]. The two types are distinguished by proliferation of microtubules in the distal dendrites between chemo- and mechanosensory neurons [10]. This

report focuses on the role of the mechanoreceptional setae on the first antennae in sensing hydrodynamic disturbances [11]. The mechanosensory process which triggers copepod's various behaviours is shown in Figure 1-3 [12]. The mechanoreception of seta starts when the hydrodynamic disturbance induced by the environment/organisms surpasses the physical threshold of seta deformation [13], which bends the seta to certain extent. This causes a neural signal to be triggered [14] and when this signal exceeds the physiological threshold, a behavioural response is elicited based on the type of signal produced .

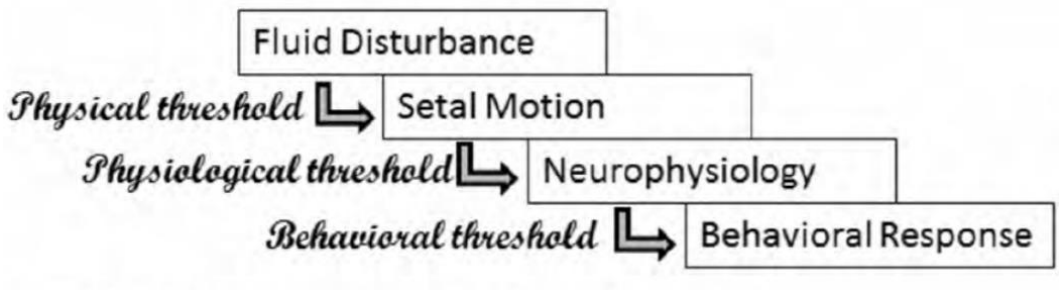

Figure 1-3 A copepod's sequence of process for behavioural response. Adopted from Fields. [12]

The mechanosensory capabilities of copepods allow them to acquire information from the surroundings and trigger certain types of behaviour. Copepods generally have three common behaviours which are, predating, escaping from predators and mating [15]. When in search for potential mates, the males rely on chemoreception to follow the trail left behind by females [16]. Mechanoreception allows copepods to detect the hydrodynamic disturbance created by either prey or predators. The mechanosensory mechanisms can translate these signals to tell the size of its prey/predator, and even the three-dimensional location [17]. Thus, the copepod reacts accordingly by eliciting an attack on its prey or an escape response away from predators [18]. These behavioural processes show that copepods rely heavily on their mechanoreceptors which are setae on its first antennae for their survival.

1.3 Research Objectives and Scopes

This study aims to investigate the mechanical properties of setae on the first antennae, by utilising a flow to analyse setal deformation's threshold which triggers the predatory and escaping behaviours of copepods. The above-mentioned objective is achieved by,

1) Experimentally quantify the morphologies of setae on the first antennae
2) Experimentally determine the deformation of setae subjected to siphon flow

1.4 Report Organization

This report is organized into a few chapters. Chapter 2 covers literature review on copepods' sensory system, structure and properties and mechanical properties of structure and appendages. Chapter 3 covers the experimental method and set up used to investigate and attain results to quantify the deformation of setae. Chapter 4 lays out the morphological results, focusing on the first antennae and setae on it. Next, Chapter 5 discusses the deformation results obtained through the experimental runs. Lastly, Chapter 6 compares the estimated spring constants among setae in the three main segments of the first antenna, before ending the report with a conclusion of this study.

2 Literature Review

In this chapter, previous work on capabilities of mechanoreceptors of copepods, and investigations of the bending mechanics of setae are reviewed in this section.

2.1 Siphon Flow

A siphon is a device which is used to transport fluid from one source and displaced to another location. Traditionally, siphons are used to transport fluid upwards with the use of a pump for suction, then the fluid flows downwards in the lower section of the pipe or hose that utilizes the force of gravity. This application has been used for centuries, with one of the oldest applications was used to extract wine from a large barrel to separate the wine from impurities at the bottom of the barrel.

The Siphon Effect is governed by the Bernoulli's equation as an approximation to an idealized siphon flow,

$$\frac{v^2}{2} + \text{gy} + \frac{P}{\rho} = \text{C} \tag{2-1}$$

where v is the fluid velocity, ρ, g , y and P are the fluid density, gravitational acceleration, elevation and pressure, respectively.

With the application of a siphon flow, the flow in the siphon device can be defined in an experimental study.

2.2 Morphology of the First Antenna

It is important to establish the morphology of a copepod to understand its reactions and behaviours. The copepod's morphology has been studied thoroughly for many years. For a typical first antenna of a copepod, the antennal segment can be divided into three parts, proximal, middle and distal. The types of setae along the antenna also differs depending on the species. There can even up to four types of setae on the first antennae, such as : 1) feathered shape 2) short with rounded tip 3) short and tapered (< 100 microns) 4) long and tapered (200 – 500 microns) [19]. A past study investigates the mechanoreceptors on the first antennae of a calanoid type copepod, *Pleuromamma xiphias (P. xiphias),* using Transmission Electron Micrograph, established good structure-function relationships of these mechanoreceptors [20]. In Figure 2-1, *P. xiphias* has a first antenna with 23 smaller segments. The proximal section of the first antenna is usually more densely filled with setae. In reference to Figure 2-1, in the middle section of the antenna, the setal arrangement becomes more regular with two to three setae on each small segment. The distal tip can contain a few types of setae, generally, with longer types that can be up to 1 millimetre long [19, 21, 22]. Past studies have also found that for the same species of different sex, their setal arrangement can differ on the different smaller segments on the first antenna [19]. Lengths of individual setae differs for different species, and some calanoid copepods have setules grown on the spiniform setae [10]. Figure 2-2 shows the first antenna of another species, *Gaussia princeps,* capturing setae present on individual segments along the antennae from the proximal to the distal side [23]. For this species, the proximal segment is not too densely populated with shorter setae, and the other segments have only about one seta at each individual segment, with exceptionally long setae at the distal tip [23]. Comparing the two species of copepods above, it is clear the morphology on the first

antennae can differ significantly with the types of setae [24] and how they are populated on the antenna.

Figure 2-1 First antenna of *Pleuromamma xiphias* showing individual segments and attached setae. Adopted from Yen et al. [19]

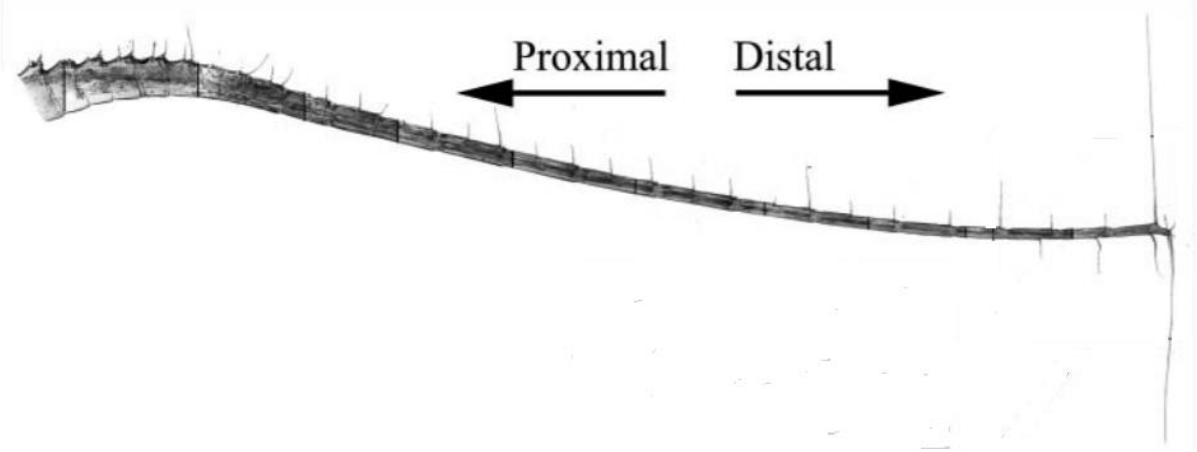

Figure 2-2 First Antenna of *Gaussia Princeps*, showing setae present on from proximal to distal sections. Adopted from Fields et al. [23]

2.3 Anatomy of Sensory System

The anatomy of the mechanoreceptors of copepods have been studied to understand how their neurological cycle works, in relation to a stimulus or disturbance encountered in their natural habitat [25]. Through investigations, the study claims the rigidity of the

receptor limits the elasticity, where compliance between seta which is movable and the stationary antennal segment is decreased [26], enabling the copepod to pick up high frequency signals. Through their study [20], they found that the distal dendrites are linked with four accessory cells, scolopale, anchor, inner and outer sheath cells as illustrated in Figure 2-3. Each sensory seta contains a scolopale and two other sheath cells that surrounds the dendrites. The anchor cell nay be shared by several sensory setae. One of the significant morphological features is the large number of microtubules surrounded by the scolopale tube and is firmly anchored to the cuticle. These microtubules fill the distal dendrites which are within the first antennae, where the scolopale tube completely encloses and is firmly attached to the cuticle.

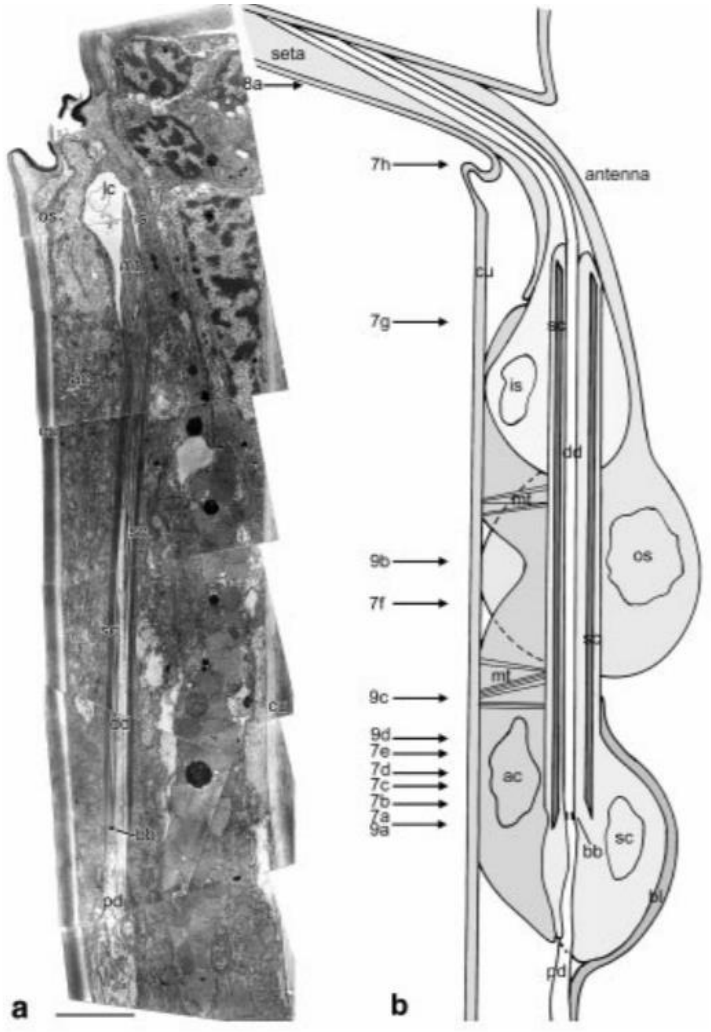

Figure 2-3 Elements of Mechanoreceptors of *P. xiphias* a) TEM of the longitudinal section of the antennal segment b) Schematic drawing showing antennal mechanoreceptor and the positions of sensory dendrites and enveloping cells. Adopted from Weatherby et al. [20]

A scolopale tube is made up of fibrillar, electron-dense substance with anti-actin anti-bodies, similar with other crustaceans. The scolopale tube contributes to the rigidity as a supporting structure partly due to the thickness, geometry and length of the tube. In addition, the firm anchoring of the scolopale to the cuticle of the antenna, with microtubules attachments, further ensures the rigidity [20].

Morphological studies have substantiated that the setae on the first antennae are important sensory structures that has mechanoreceptive capabilities [27], with the presence

of sensory cells in the first antennae [28]. In the morphological study by Yen et al. 1992 [19], muscle tissue was found to be present along the antenna, suggesting that calanoid copepods can control the movement of the antenna to a certain extent. Further studies on the behaviour and neural responses are also done to understand the mechanosensory system of copepods, and to establish a structure-function relationship.

2.4 Mechanosensory Mechanism

Mechanoreceptors of copepods are found mainly on their first antennae, which are responsible to detect any fluid signal indicating nearby planktonic prey, predators or potential mates, where they react accordingly. Copepods operate in the range of millimetres and milliseconds, thus, their sensorimotor performance exceeds most of the arthropods [19, 29, 30]. In the calanoid order of copepods, they detect predators using multiple mechanosensory setae on their first antennae [29, 31, 32]. The setae attached on the antennae pivots on a basal hinge and bending of the setae triggers the mechano-gated ion channels which are part of the sensory neuron's membrane [10]. These mechano-gated channels are claimed to be connected by linking proteins inside and outside of the sensory cells [33]. When setae bends, a tension is formed on the links which open the channels which excites a behaviour according to the signal received [10]. Thus, a copepod relies on its mechanoreception capability to detect fluid disturbances in the surroundings [34] [35] by their mechanoreceptors linked to the setae found on the first antennae [20].

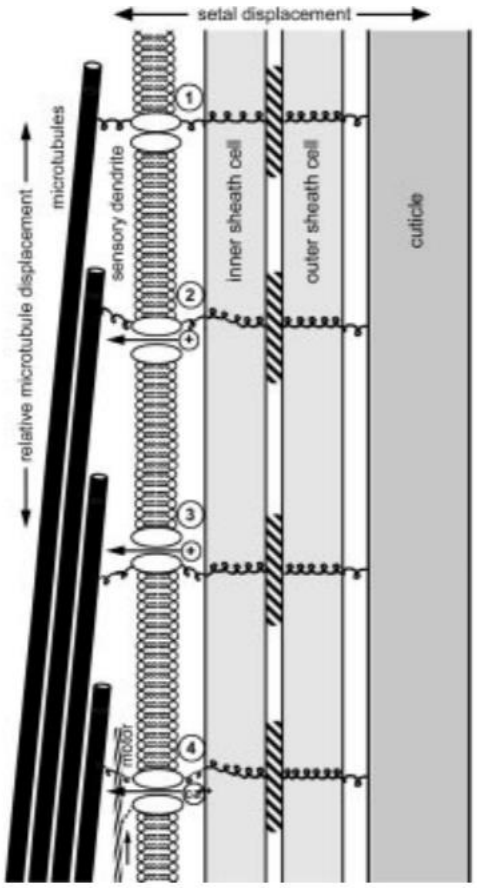

Figure 2-4 Model of a Copepod's Mechanosensory System. Adopted from Weatherby et al. [10]

Figure 2-4 above portrays a model for a copepod's mechanosensory system based on ultrastructure and analogy to molecular mechanisms in other systems [36]. These features such as the sensory dendrites are within the first antennae, which terminates at the root of its setae [20]. Within the seta, sensory dendrites are enclosed by inner and outer sheath cells, which terminates together with its microtubules by firmly anchoring to the setal cuticle. The support from the microtubules and attachment to the cuticle gives rise to the rigidity of each seta. Rigidity of the receptor may limit its elasticity and decreases the movement of setae, which enables detection of high-frequency giving it enhanced mechanical sensitivity [10].

2.4.1 Directional Sensitivity

From Figure 2-5 below [37], the model explains that the bending of setae in either direction can cause tension on and dendritic membrane to elicit a neural signal. Predating and making escapes from predator do not only require detection of the magnitude of the hydrodynamic disturbance, but the direction matters as well. A proximal and distal deflection of the setae results in an asymmetry response physiologically, shows a certain extent of directional specificity [12]. Morphological features on the first antennae may be the cause of these effects. For a case where the cuticular socket which holds the seta restricts motion in a certain direction can elicit a response which is directionally biased [38, 39]. These features can result in seta having higher rigidity in one direction than the other. Setae with single innervation are unlikely to detect accurately in relation to directional signals with a single seta [12]. A single mechanoreceptor depends on both magnitude and direction of the hydrodynamic disturbance, and different combinations of these two factors can elicit the same neural response [1, 40]. However, detection from various setae eliciting signals can be a good mechanism for spatial location [12]. The delays in trigger of the neural signal of adjacent setae can evaluate the speed of disturbance and its direction, as the order of the triggered signal from each seta distinguish the direction [41].

2.4.2 Physical Response

Understanding a copepod's mechanosensory behaviour requires analysis of the physical response of the sensor when subjected to a fluid disturbance. An experimental study on a species Gaussia princeps [41] uses water jets to stimulate response from the copepod's mechanosensory setae. Different setae on the distal segment of the first

antennae was monitored by subjected to the water jets. Displacement of its setae was found to increase with increasing speed of the water jet. However, each seta has different amount of resistance to motion, thus, their angular displacements differ when subjected to fluid disturbances. The morphology of setae affects the physical response when subjected to water jets at different directions. For *G. princeps*, angular displacement towards the distal direction was found to be two times the displacement when displaced towards the proximal direction at the same speed. However, not all setae showed the same difference of displacement in these directions. This explains not all setae have a directional bias in terms of physical response.

2.5 Experimental Quantification of Setal Sensitivity

It is important to quantify setal sensitivity by means of experimental studies that observed displacements of setae of the first antennae either through methods of artificial stimulus [42] or using live prey. Copepods are highly dependent on their ability to adapt to their surroundings, reacting to nearby prey, potential mates and approaching predators [43, 44]. They rely on ambush feeding most of the time to capture their prey which explains the high success rate, where mechanoreception is the main mechanism for this process [43]. Most studies focus on the setae of copepods which have mechanoreception capability because they are significantly affected when they are subjected to hydrodynamic disturbances near the body and setae.

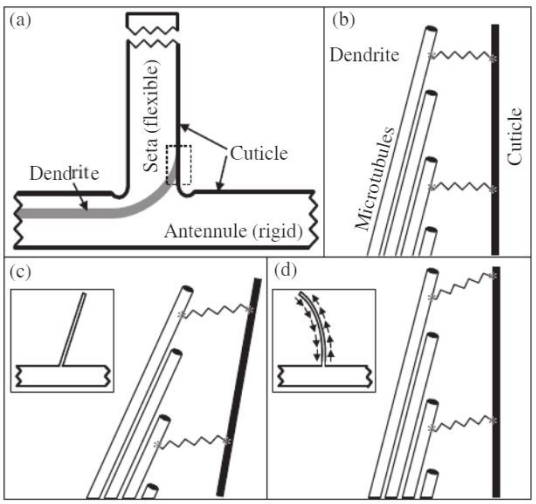

Figure 2-5 Proposed model for Seta Deformation and Transduction Process. Adopted from Shen et al. [37]

Setae on the first antennae are subjected to hydrodynamic disturbances which causes bending of the setae, a transduction process occurs in the mechanosensory dendrite that is attached to the cuticle at the setal root [10, 20]. In Figure 2-5(a) above, it depicts the sensory dendrite within the antenna which terminates at the setal root that is attached to the inner wall of the cuticle. The microtubules within these dendrites are connected to the cuticle through fibers and dendritic membrane which are represented by the spring labels. (Figure 2-5(b)) When the setae is bent due to hydrodynamic disturbances, it causes the cuticle to displace and the dendritic membrane is pulled in tension [37]. (Figure 2-5(c)) Thus, this results in the opening of mechano-gated channels which triggers a neural signal for the copepod to react. Similarly, in Figure 2-5(d), when the setae are bent in a curved manner to the left, it compresses the left cuticle and the right cuticle is pulled. This leads to a shear displacement of the cuticle, resulting in tension of the dendritic membrane. Generally, when seta bends and causes a displacement of the cuticle, the tension on the dendritic membrane causes an ionic flow across the mechano-gated channels and triggers a neural signal. Thus, the sequence of events for a behavioural response starts from a hydrodynamic disturbance,

which leads to the deformation of setae that is enough to trigger a neurological signal for it respond as depicted in Figure 1-3 [12] .

2.5.1 Artificial Stimulus

Experimental studies have been carried out to understand the behavioural and neurological responses of copepods when setae on its first antennae are subjected to hydrodynamic disturbances. One of the first studies on this used recording of the nerve impulses transmitted along the first antennae of calanoid copepods. This neural signal is elicited with the forceps connected to a transducer causing vibrations [19]. This method was adopted again but improved to induce a natural stimulus onto its setae without direct contact with the transducer. The transducer has an extra connection of a sphere submerged into the same medium as the copepod's antenna. A dipole pattern of water displacement is created to stimulate its mechanoreceptors. (Figure 2-6) The copepod was held by a forceps electrode and submerged into mineral oil, leaving the distal and middle portion of the antenna in sea water beneath the plastic ring. The oil prevents current flow where the body and proximal portion of antenna is submerged in. As the transducer causes hydrodynamic disturbance in the sea water, the electrical potential across the electrode and seawater which is grounded, is induced by a neural signal elicited due to the disturbance is recorded by their recording system. From the experimental study by [45], it shows clearly that setae on the first antennae are sensitive to hydrodynamic disturbances which elicits neural activity.

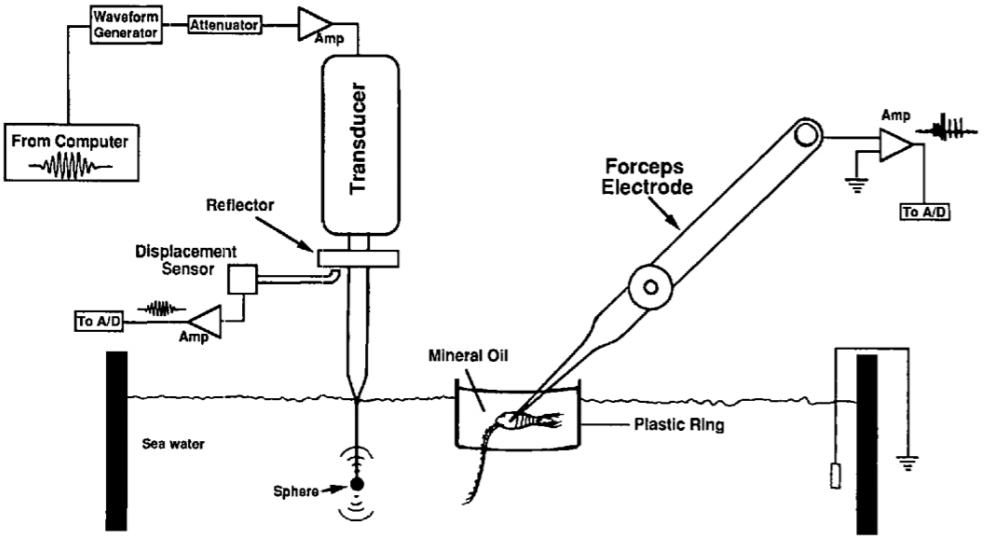

Figure 2-6 Schematic Diagram of Experimental Set up using a transducer to induce vibrations that elicit response from the copepod. Adopted from Yen et al. [19]

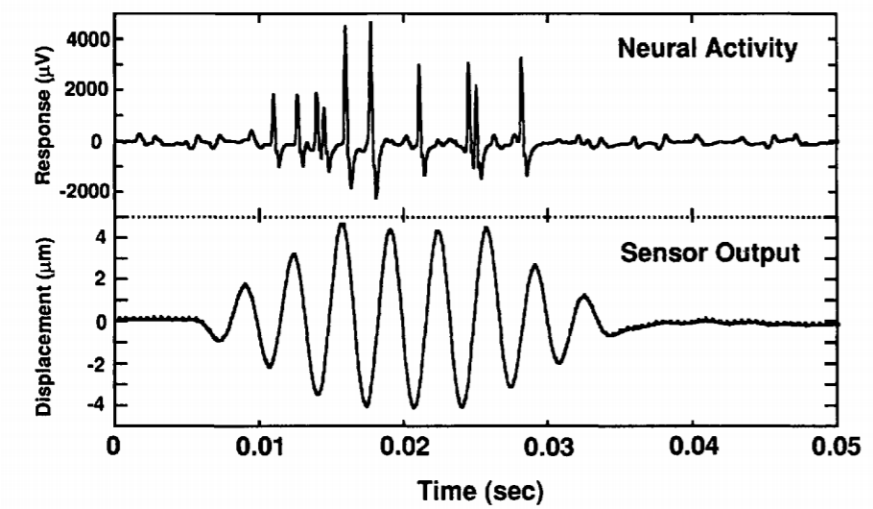

Figure 2-7 Experimental Results of Mechanical Stimulus to elicit neural response from calanoid copepod, Pleuromamma xiphias' first antennae setae. Adopted from Lenz et al. [45]

In Figure 2-7 above, it shows the neural activity when subjected to mechanical stimulus from the transducer's vibrations in terms of displacement of the stimulator. The neural activity is proportional to the displacement of the stimulator, recording a peak 4000 μV at a displacement reading of about 2 μm at 0.015s with the stimulator vibrating at a frequency of 300 Hz.

In another experimental study, individual setal deformation was successfully recorded for the first time, belonging to the first antenna of *Gaussia princeps*. This study was able to capture the angular displacement of four individual setae and investigated its physiological response when stimulated by a water jet [41]. Setal displacement is shown clearly in Figure 2-9 when subjected to the water jet stimulus, showing the original position A to its maximum displacement position. Each labelled position is the displacement recorded at intervals of 2 ms for the period when the valve remains open. In this experiment (Figure 2-8), amputated antennule was used instead of the whole copepod which was easier to position. Water jets were used to stimulate the individual seta by a micro-injection system (Picosprizter II) which shot jets out of the pipette by compressed air at a pressure of 344 kPa. The timing and speed of the water jet was controlled by a timer which opens and closes the solenoid valve. In Figure 2-10, the water jet only exits the mouth of the pipette after being triggered for approximately 20 ms. It accelerates upon exiting and the head speed increases to its maximum after some distance from the pipette mouth. Subsequently, it decreases in speed due to interaction with the stationary fluid. The physiological responses were recorded as setae were subjected to these water jets proximally or distally by the forceps grasping the antennule which is connected to a neural signal detection system [41].

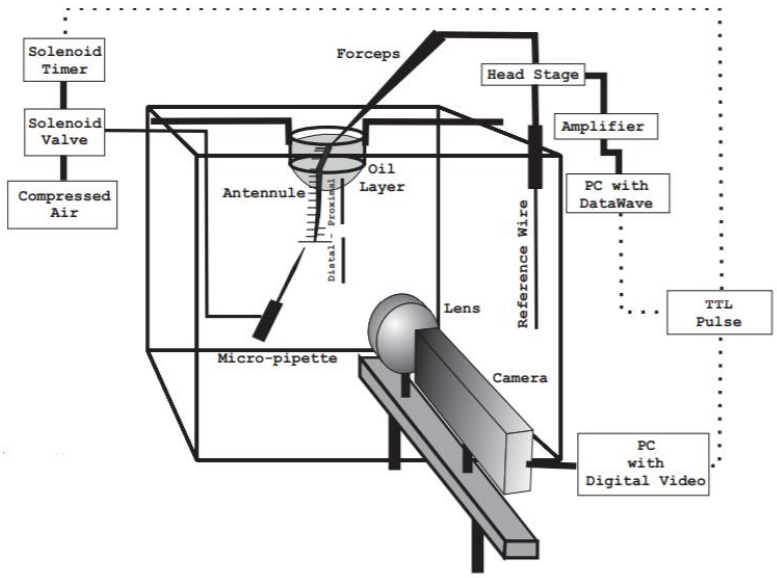

Figure 2-8 Schematic Drawing of Experimental Set up using Water jet to stimulate suspended antennule. Adopted from Fields et al. [41]

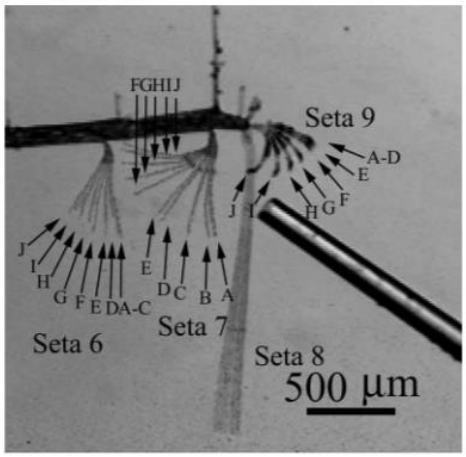

Figure 2-9 Individual Setal Angular Displacement of first antennule of Gaussia Princeps. Adopted from Fields et al. [41]

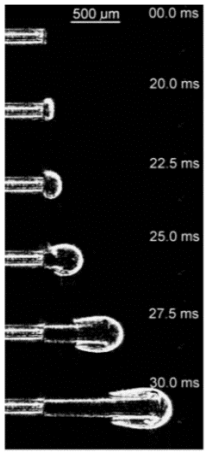

Figure 2-10 Time Series of Water Jets shot out of Pipette , showing water expelled out of mouth only after 16 to 2ms (Recorded at 2000Hz using Schlieren optical pathway) Adopted from Fields et al. [41]

As seen from graphs A & B in Figure 2-11, Seta #8 (Distal) shows ultra-sensitivity with a strong response although subjected only to a small water jet speed. A shorter Seta #7 (Figure 2-12(a)), is not sensitive to hydrodynamic disturbances as does not provide consistent responses. This study was able to characterise the responses from individual seta when subjected to respective water speeds.

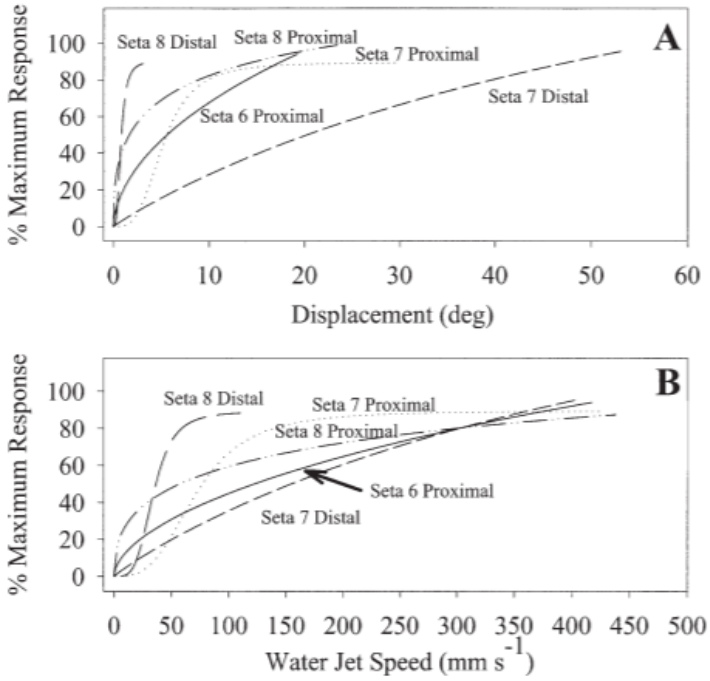

Figure 2-11 Physiological Response of individual mechanoreceptors subjected to water jet stimulus. A: Response as a function of Angular Displacement B: Response as a function pf water jet speed. Adopted form Fields et al. [41]

2.5.2 Stimulus by Real Prey

Copepods use their mechanosensory mechanisms to detect prey that are nearby. A past study has observed prey attacks executed by *Acartia tonsa (A. tonsa)* and *Oithona davisae (O. davisae).* Figure 2-12 shows the captured images of attacks and capture of its prey. In part A, it shows time frames of *O. divasae* detecting its prey as pointed by the arrow and making its approach to its capture. Parts B & C shows *A. tonsa* making its capture of its prey, the white image depicts the predator's initial position and reorients by a quick attack to its final position shown by the black image. Part D shows *O. divasae* doing a capture as well. Through observations, prey attacks are elicited when prey comes within approximately 0.2 mm of the first antennae. This distance quantifies the sensitivity of these 2 species where the flow disturbance created by the prey is picked up by bending of the setae on the first antennae within this distance [17].

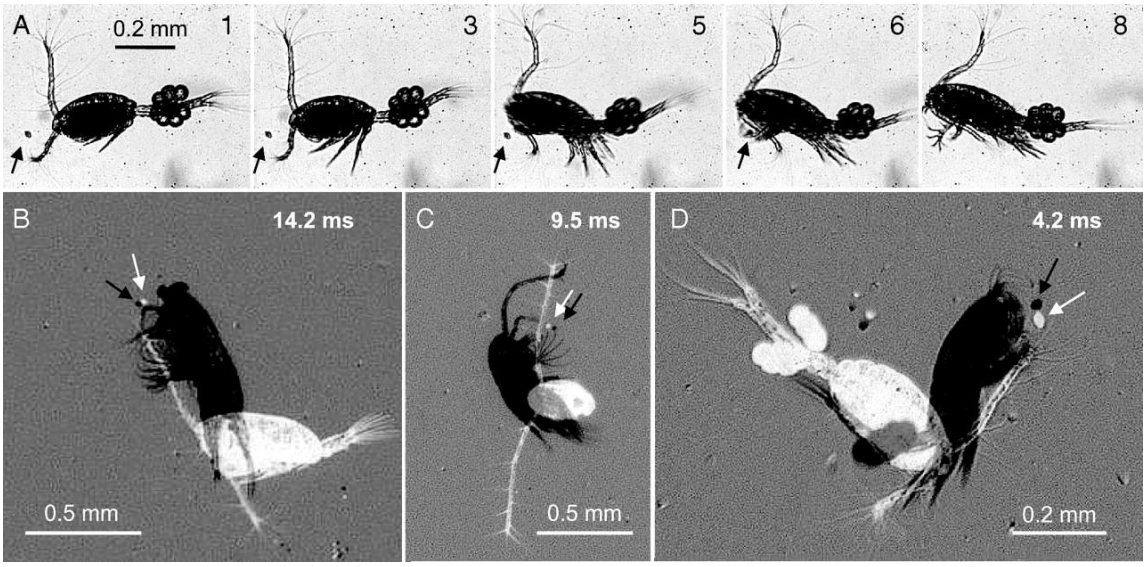

Figure 2-12 A: Frames of copepods attack and capture of it prey , B-C : White image represents before its attack jump, and the black image shows its orientation after attacking (A&D:O .divasae , B&C:A. tonsa) Adopted from Kiorboe et al. [17]

The key to a successful attack of a copepod is to be able to identify the 3-Dimensional (3-D) position of its prey. Copepods are generally blind and rely on their mechanosensory setae on the first antennae to detect motile prey [46]. These setae are spread out along the antennae and these sensors allow the copepod to detect signals to determine the 3-D position of its prey, and even its velocity through hydrodynamic disturbances. When it attacks during the first few milliseconds, it is unlikely to be able to sense new information as signal sent through the antenna can about 2-10 milliseconds. Thus, its sensors are sensitive enough to give a precise position on the initial attack [47].

2.6 Numerical Models of Mechanical Properties

This section discusses some past studies which utilise numerical models to estimate mechanical properties of setae on a copepod's first antenna.

2.6.1 Estimating Young's Modulus

Many studies have investigated a copepod's physiological and behavioural responses, numerical studies also add on substantiate results from past work. A numerical study by [48], attempted to evaluate if mechanosensory setae on the first antennae of copepods can detect pressure changes by estimation of mechanical properties. Additionally, a biomechanical model (Figure 17) was used to estimate the deflection of seta at a certain pressure difference. The Young's Modulus (E) of seta was estimated based on values of Young's Modulus of protein present in copepods from past studies [49]. One of the values was based on keratin, $E_{keratin} = 3 \times 10^3$ MN/m^2 [50], and the other based on resilin, $E_{resilin} = 10$ MN/m^2, where these values differ more than a hundred folds [48]. Thus, the estimated value based on a seta that is 2 – 5 μm thick, $E_{seta,estimated} = 100$MN/m^2 , which was in between the values of the two types of protein. The estimated value was then used to find the value of Shear Modulus (G) as well, $G_{seta,estimated} = 3.85$MN/m^2 . In conjunction with these estimated values was a design of a biomechanical model as shown in Figure 2-13, to find the minimum pressure difference that will trigger a neural response. Through their analysis and model, in order to detect a 50 μm particle, the seta would have to be 2 m long. Therefore, the study concluded that the mechanoreception capability of copepods was unable to detect pressure difference, together with the assumption of an inadequate biomechanical model used for the analysis [48].

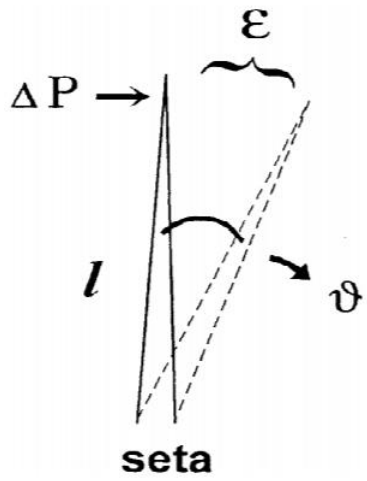

Figure 2-13 Biomechanical model of seta deformation with pressure change. Adopted from Yen et al. [48]

The experimental studies discussed above focused mainly on behavioural and physiological responses which were elicited based on artificial stimulus. The relationship between hydrodynamics disturbance and neural response was characterised in these studies with different experimental methods, such has quantifying neural response at different water displacement [51], and characterising physiological response of individual seta when subjected to an angular displacement [41]. For the study based on numerical analysis [48], it was the first to estimate mechanical properties of seta on copepods. However, there are some limitations to these investigations. Firstly, there was lack of focus on the physical threshold displacement of setae to trigger a neural signal. Secondly, an estimate of mechanical properties of seta based on two types of protein that is present in a copepod is not an accurate representation. Thus, the work described above is not adequate to explain the physical deformation threshold limits of setae and its mechanical properties.

2.6.2 Quantifying Setal Deformation

Displacement of setae on the first antennae can be quantified by two ways, 1) Angle between its initial and final position, 2) Distance it has displaced from the original position. Firstly, when seta on the first antenna bends with a certain degree of curvature (Figure 2-8(d)),

the difference of the initial and final angle can be quantified. Secondly, seta may only bend at its base without any curvature (Figure 2-8(c)), so it is possible to quantify the displacement distance from the seta's initial to final position [37]. A past study by Shen et al. 2020 [37], defined numerical models based on Resistive Force theory to find forces on seta due to hydrodynamic flows, as well as Euler beam theory to find the deformation of seta when subjected to those forces.

2.7 Responses to Prey and Predator

Many studies have been done to understand a copepod's behaviour, especially on ambush feeding and escape responses from approaching predators. These studies [52] help to establish an understanding of their common behaviours in their natural environment.

2.7.1 Motile and Non-Motile Prey

There are different types of prey that copepods go after which may be moving or stationary. Small cruising zooplankton like copepods rely on remote prey detection and capturing of active prey for satisfactory feeding [43]. In a study of prey detection, it presents a novel mechanism for prey detection in a moving copepod. Both motile and non-motile prey can be detected by the cruising copepod, but the two types were detected at different positions from the copepod. The two types of prey used in this study, 1) Copepod Nauplius (Motile Prey) 2) Dinoflagellates (Non-Motile). In Figure 2-14(a), shows a situation of the predator, *Metridia longa (M. longa),* detecting the prey which is the nauplii of *Acartia Tonsa*. The prey tries to make an escape jump and the predator picks up the hydrodynamic disturbance that elicits an attack jump, subsequently using its feeding appendages to draw in the prey for successful

capture. For a case of non-motile prey (Figure 2-14(b)), the dinoflagellate was only detected by the predator after passing it, and the attack was only triggered when it was near the feeding appendages or second antennae of *M. longa*. Thus, the predator detects motile prey through hydrodynamic disturbances that copepods are sensitive to when it makes an escape jump, and for non-motile prey, it has to be in the region of motion of the feeding appendages or second antenna that is about 1 mm wide [43]. This study explains how cruising copepods survive in their habitats with these feeding modes.

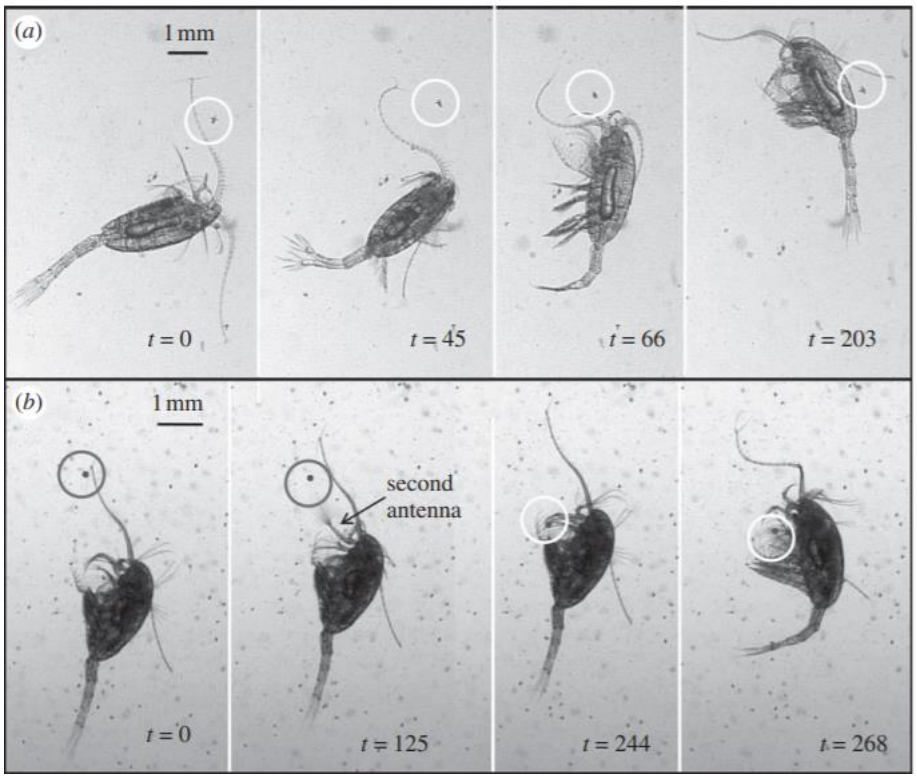

Figure 2-14 Time Frame for Detection of Prey a) Copepod Nauplius b) Dinoflagellate. Adopted from Kiorboe. [43]

2.7.2 Predators

Predating is another main behaviour of a copepod, however, they are not always the predator in some cases. Zooplankton feeding at the food-rich surface layers of the ocean are at higher risk of exposure to its predators [53]. Many animals are both positions of being the prey

and predator of others, thus, the gain from predating has to be compared with the risk of being eaten [54]. The general pattern that shows is that the copepod tends to elicit as escape response [55] when it detects a flow disturbance produced by a bigger organism. How this process happens is when the predator approaches the copepod and the which causes a fluid disturbance and becomes entrained in this feeding current [54]. The mechanosensory system of the copepod picks up this deformation and a neural signal is triggered for escape behaviours. Once a predator is detected, they are capable of sequentially using their swimming legs to accelerate off up to a velocity of 500 body lengths per seconds within milliseconds. Thus, a copepod is able is detect the distance and speed of its predator from the fluid signal, and once the deformation is above its threshold rate [56], it elicits an escape response.

2.8 Research Gap

The studies done till date have focused much on investigating the physiological responses of copepods when setae on the first antennae is bent due to hydrodynamic disturbances. There is a lack of experimental study on the physical deformation threshold rate of setae when subjected to hydrodynamic disturbances. Thus, it would be feasible to set up an experimental study by subjecting the setae on the first antennae to a Siphon Flow.

3 Experiment Set Up

This chapter discusses the current experimental method, including a culture set up of copepods as a source of specimen for experimental purposes and to explain the experimental process utilizing necessary devices and apparatus.

3.1 Copepod Culture and Preparation

The specimen used in this experimental study is *Pseudiaptomus annandalei (P.annandalei)* is cultured for future experimental purpose. *P.annandalei* is a type of calanoid copepod with adult size ranging from 800 to 1000 micrometres, which is feasible for this study's experiment. *P.annandalei* is obtained from a local supplier that farms copepods locally. The culture is maintained and cultured as shown in the basic set up in Figure 3-1.

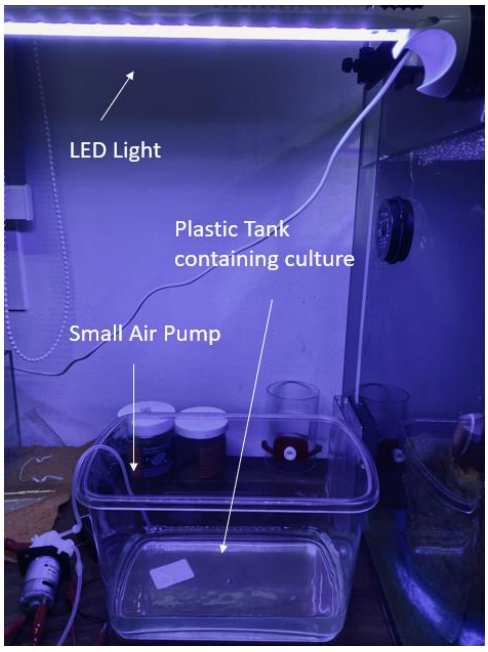

Figure 3-1 Culture delivered into a small plastic tank

The original source of *P. annandalei* is transferred to an open tank where the fresh culture is kept in, exposed to LED light which is necessary for copepods to grow and reproduce for 12

to 16 hours a day. A small air pump is kept running for 2 to 3 hours each day to supply the water medium with air at a low rate with 1-2 bubbles/second. Approximately 5 mL of phytoplankton is introduced on alternate days as their food source. The culture is maintained by rinsing the existing eggs, nauplii and adult specimens into a tank of fresh filtered seawater on a bi-weekly basis.

3.2 Experimental Design & Set Up

A simple set up is utilised to establish certainty of setal deformation which can be observed under the microscope. The design of this experiment is kept to minimal apparatus, with the focus to capture deformation of setae on the first antennae of *P.annandalei.* The main apparatus used for this set up consists of a syringe pump, 10 mL syringe with tubing of 0.51 mm diameter, microscope, petri dish with water and a pair of forceps (Figure 3-2). The pair of forceps has a small tip of 0.1 mm as it requires much precision to accurately grasp the body of the adult *P.annandalei* which is barely visible to the naked eye.

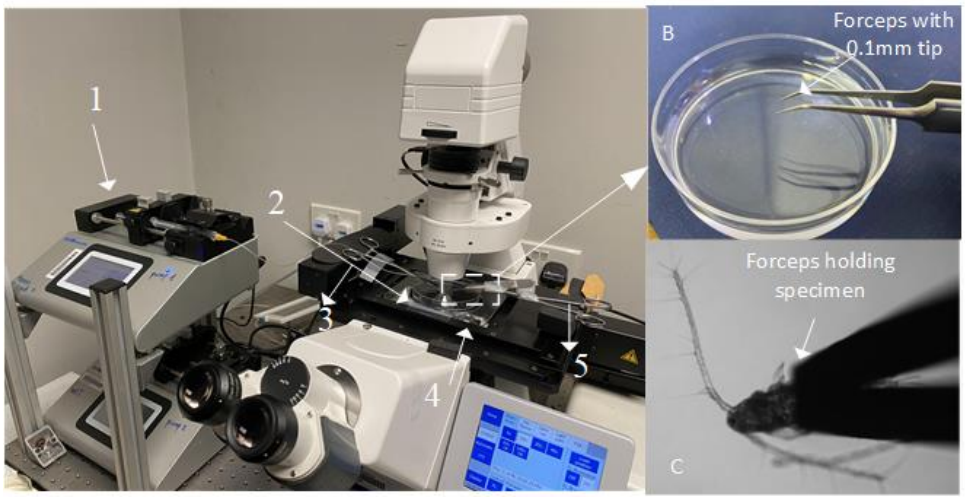

Figure 3-2 a: Experimental Set-Up consisting of 1) syringe pump, 2) petri dish containing water, 3) forceps holding tube connected to syringe on the syringe pump 4) objective of microscope to observe setal deformations 5) forceps tip holding body of copepod specimen Figure 3-2 b: Forceps with 0.1mm tip to pick out copepod specimen contained in a petri dish Figure 19c: Forceps successfully grasped onto body of copepod

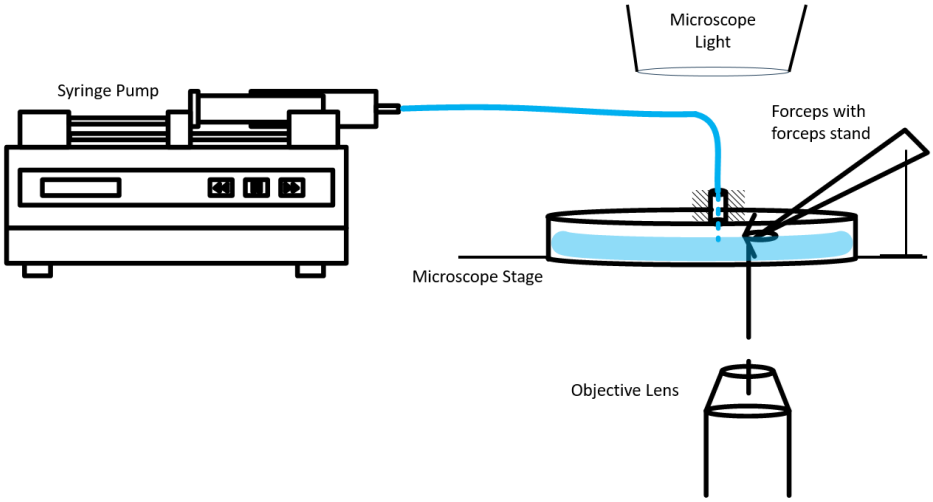

Figure 3-3 Schematic Drawing of Experimental Set-Up showing the connections between the syringe pump and running tube to the petri dish on the microscope stage, with the specimen clamped by forceps in line with the objective lens

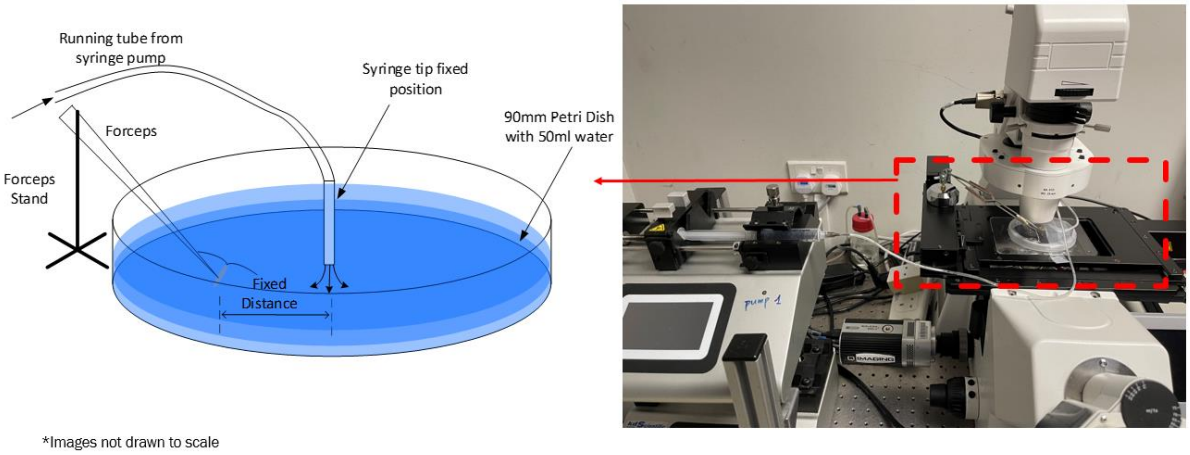

Figure 3-4 a: Schematic Drawing of Tube direction showing flow output perpendicular to orientation of setae of the first antennae from the copepod specimen, with its position affixed by a pair of forceps. Figure 3-4 b: Observation under the microscope showing flow direction perpendicular towards setae present on first antennae of copepod clamped by forceps

In Figure 3-3, it shows the schematic illustration of the experimental set up where the left of the image shows a 10 mL syringe attached to the syringe pump with a running tube. A pair of forceps holds the end of the tube outlet to adjust the direction of output when submerged in water contained by the petri dish. The end of this tube is submerged into water contained into the petri dish, where the setae on the first antennae will be subjected to this flow. On the

right of the microscope's stage, the copepod specimen is clamped by a pair of forceps holding the body down and submerged into the water. The rubber tube connected to the syringe ends with a syringe tip termination seen in Figure 3-4(a), which is fixed onto the top cover of the petri dish to ensure the position of the outlet is constant in each experimental run. Half of the cover of the petri dish is cut out to allow space for the forceps to place the copepod specimen in the water contained within the petri dish.

3.3 Experiment Process

The experimental setup above aims to investigate deformation of setae on the copepod's first antenna when subjected to an artificial stimulus (Figure 3-3). Firstly, the copepod is aligned such that the seta on the first antenna is perpendicular to the flow from the outlet submerged in the same medium, where this flow causes the seta of interest in that particular run to bend towards the distal end of the first antenna. The syringe pump holds a 10 ml syringe containing water, pushing this water out through the termination tip to provide artificial stimulus. The flow rate through the outlet is controlled by configurations in the syringe pump's software.

After setting up the flow rate and pattern as shown in Figure 3-5, the deformation process of seta is observed and being recorded using a PCO high-speed camera. The deformation process is recorded in frames at 60Hz so the displacement of the seta can be thoroughly analysed. The deformation is observed at different output flow rates of 10mL/min, 15ml/min and 20ml/min. Figure 3-5 depicts how the flow is introduced into the same medium where the copepod is submerged in as an artificial stimulus. For example, for the flow rate of 10 mL/min, the flow linearly increases to the desired flow rate in the first 3 seconds, then held

for 5 seconds to allow setae to be displaced to its final and steady position, and decreases linearly to 0 in the last 3 seconds. This method of injecting flow from the syringe is conducted for each flow rate. After capturing the distal bending for the three flow rates, the same steps are repeated to observe proximal bending of the same seta. This is done by placing the specimen on the other side of the outlet, taking reference from the initial position for distal bending. The two directions of deformation are observed to analyse and define directional sensitivity of setae on the first antennae. The flow rates adopted for observing both proximal and distal bending are the same to allow a fair comparison.

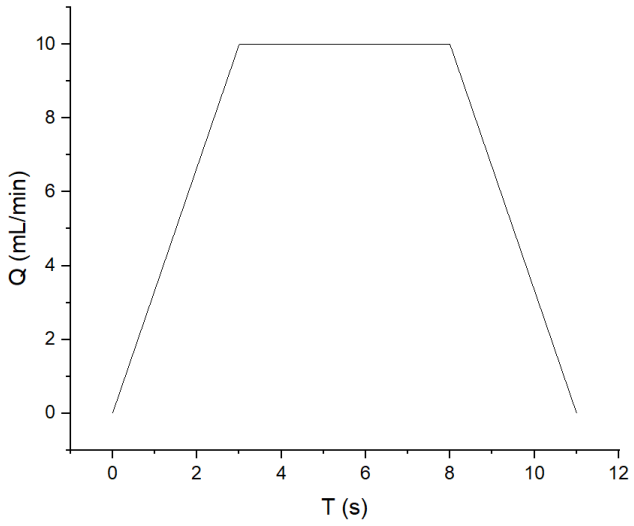

Figure 3-5 Flow Rate (Q) vs Time (T) Graph depicting output flow rate from syringe pump, taking the first 3 seconds to reach the desired flow rate and held for 5 seconds, and gradually decreases to 0 in the last 3 seconds

4 Morphological Quantification

4.1 Setal Morphology

In this section, the author quantifies the morphology of a group of adult *P. annandalei*, specifically its first antennae and the lengths and types of setae present on the first antennae (Figure 4-1). This species was chosen based on its body size and antennule length for the feasibility of this experimental study as the body size needs to be large enough to be grasped with a pair of forceps. The observations show that the prosome length of an adult *P.annandalei* is 0.8 mm on average of sample specimens from the culture tank, and the length of the adult's first antennae with an average of at least 1.04 mm, having a standard deviation of 49 μm, with a diameter of ranging approximately from 47 μm on the proximal end to 20 μm on the distal end. (Figure 4-2). These observations are similar to previous literatures that have quantified the morphology of *P. annandalei* [57]. There are two types of seta found on *P. annandalei*, the smooth and long type, as well as short and tapered ones. Most of these setae can be clearly seen on the first antennae. There are almost the same number of each type of seta present on the first antennae, where the smooth and long ones are present along the antennae, and the short and tapered seta are found mainly on the proximal and middle segments. The smooth and long setae at the proximal segment of the first antennae has been observed to have a maximum length of approximately 90 μm (Figure 4-4). Yen et al reported that *P. xiphias* [19] has four types of seta, where *P. annandalei* is observed to have only two types. The difference shows that different species of copepods have different setal morphology. Moreover, from observations during the experimental process, the first antennae of *P. annandalei* is at least 1 mm in length which is longer than its prosome (Figure 4-1). The long antennae allow the copepod to have a larger area of sensing for hydrodynamic disturbances in its surroundings.

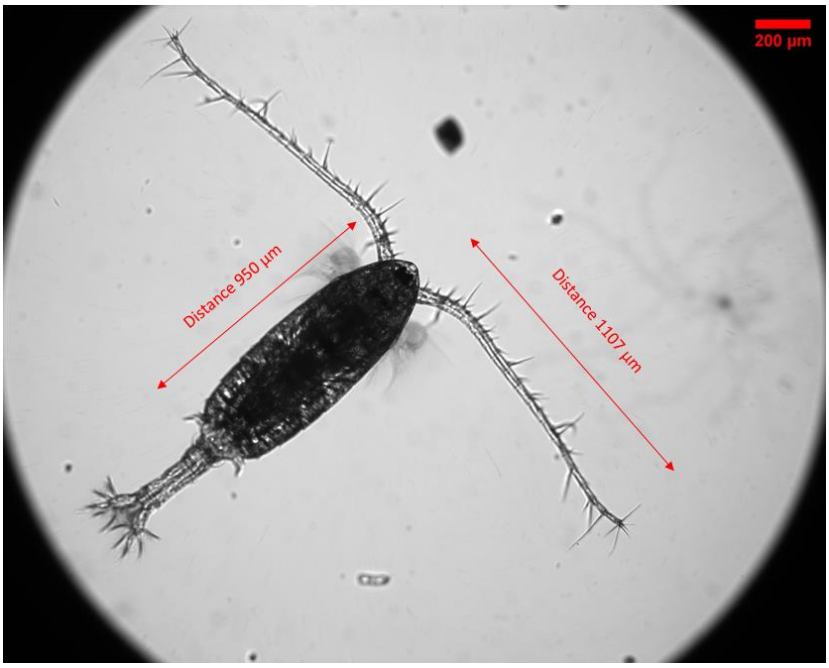

Figure 4-1 Live Specimen of *P. annandalei* observed under the microscope, as a sample taken from the culture

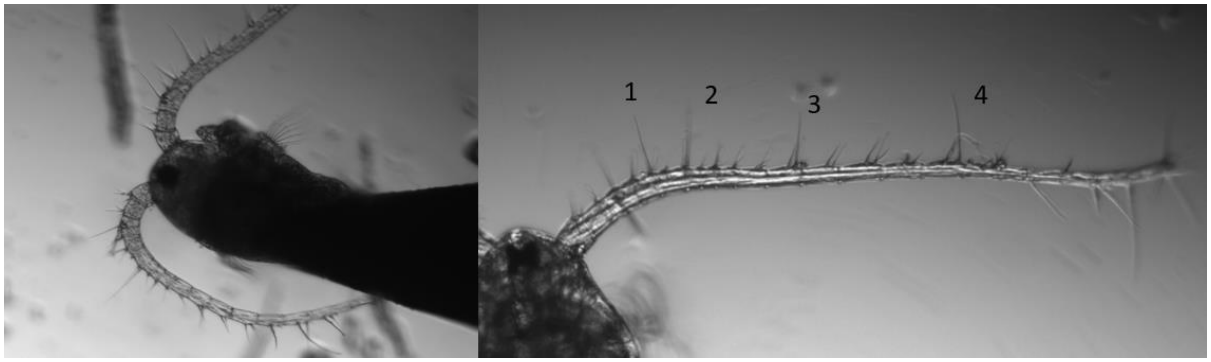

Figure 4-2 a) Left Image: Copepod clamped by forceps, showing both sides of first antennae and proximal setae. b) Right Image: Setae on the first antennae on proximal, middle and distal sections, labelled #1 to #4 for the four main long type of seta

In Figure 4-2(a), the copepod is grasped by a pair of forceps, showing both sides of the first antennae, and Figure 4-2(b) shows the four main long type of seta on the first antenna. These four setae are similar and regular that spread out along the proximal, middle and distal sections of the first antennae in this manner for the breed of *P. annandalei*. As shown in Figure 4-3 and Figure 4-4, shows measurements conducted on the specimens for the smooth and long

type of seta on the first antenna. The average length of the long type of seta on the first antenna is found to be 84 µm.

Figure 4-3 Setae along the first antenna, with measurement of long seta on the middle segment

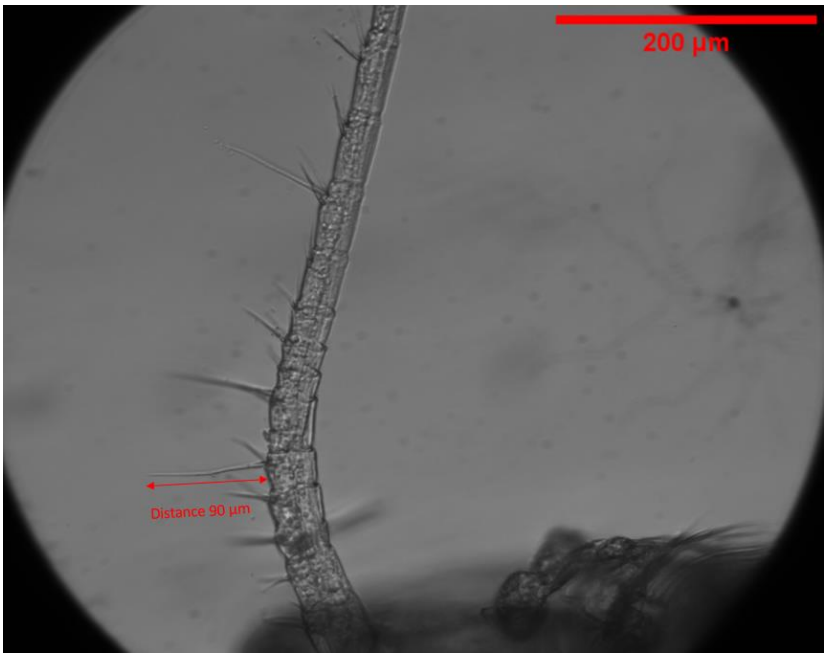

Figure 4-4 Setae on different segments of the first antennae; with measurement of long setae at the proximal end

4.2 Long & Smooth Type Seta

This study focuses on the long and smooth type of seta among the array of setae belonging to the first antennae of the *P. annandalei*. There are four main setae belonging to the long and smooth type that are quantified for the morphological section. For each seta of the four long type of setae, the setae are measured from five different specimens to gain a better insight of these lengths. Figure 4-5(b) shows a summary of the lengths for the four setae from each individual specimen. Seta #1 shows a significant range of lengths, ranging from 75 μm to 90 μm. The adjacent proximal seta, Seta #2, has a much smaller variation, with length measurements of 82 μm to 87 μm. The middle seta, Seta #3, does not have a large variation as well, ranging from 75 μm to 83 μm. Seta #4, which is the distal seta is similar to Seta #1, having a larger range of 76 μm to 90 μm.

Seta #1 and #4 shows larger variation in terms of length from the five sample specimens, and both setae have shown in the measurements to have the longest possible length on both ends. Other the other hand, Seta #2 and #3 have smaller variations from the measurements and tend to have a shorter length as compared to Seta #1 and #4.

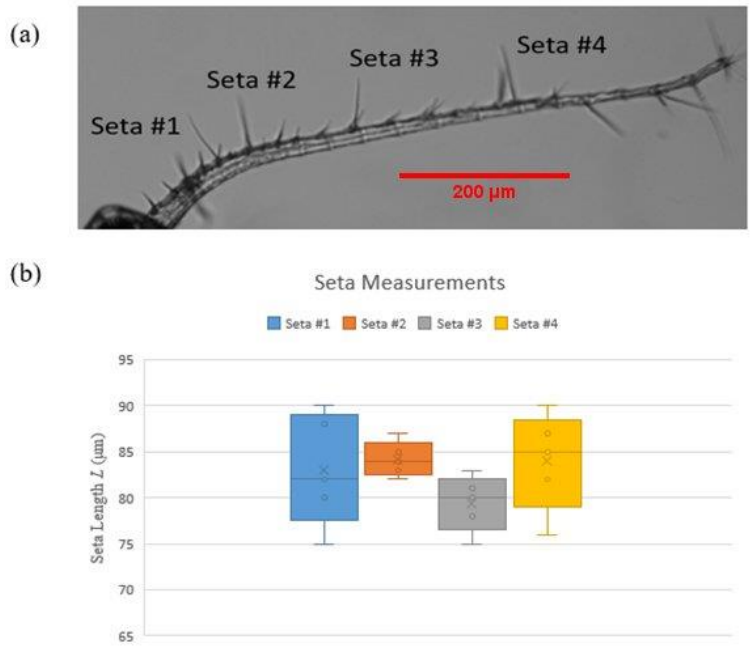

Figure 4-5 Sample Specimen Measurements of Long and Smooth Type of Seta

5 Setal Deformation

5.1 Quantifying Setal Deformation

The purpose of subjecting setae to an artificial stimulus using the syringe pump is to observe setal deformation, simulating hydrodynamic disturbances encountered in a copepod's natural habitat. The current experimental setup allows precise quantification of setal deformation and morphology present on the first antennae of *P.annandalei.* The copepod specimen is placed above the objective to view its setae on the first antennae. Before subjecting the setae to any flow, the morphology of the adult specimen is analysed by taking snap shots and recordings of the copepod's movements. With snap shots of setae from the first antennae, a scale bar is set on the microscope's software to take measurements of lengths of setae. Similarly, with recordings of the deformation of setae, the images can be processed to measure the displacement of a particular seta from its initial position to the final position when subjected to a hydrodynamic disturbance. The captured images from the high speed camera are used to

compare the initial position and the final displacement position of seta subjected to artificial stimulus at each flow rate. This process is done to analyse the maximum displacement of seta on the first antenna, and to analyse between proximal and distal bending of setae.

After each run is completed, the copepod specimen is removed without adjusting the position of the objective. The syringe is then replaced with another 10 mL syringe with a mixture of water and microbeads. Thus, when repeated with the same flow rates conducted with the specimen, the high speed camera is able to record the microbeads in this flow. The images are used to analyse the flow from the displacement of the microbeads. This process allows verification of the experimental flow conducted on the specimen.

5.2 Determine Flow Velocity by Microbeads

The exact flow velocity at the area where the seta or first antenna is, is determined by injecting microbeads into the flow. This is prepared by another syringe filled with water and microbeads, and these beads will flow into the siphon flow device. After observing the deformation of setae, the copepod specimen is removed but the objective remains in the same position. The syringe is then replaced with one that is prepared beforehand filled with microbeads. The same flow rates are executed by the syringe pump and the high speed camera will capture the microbeads that flow past the same position where the seta was. This gives an accurate depiction of the velocity or flow that the seta was subjected to during the deformation phase. The high speed camera allows different frame rates to be set to capture the flow process, thus by finding the distance between frames with the duration known, the velocity of that particular flow rate at the exact position can be determined by this method.

Figure 5-1 shows a superimposed image of a micro bead flowing pass at the focused position and depth across 5 frames, for one of the experimental runs belonging to the distal deformation segment. This process will be repeated three times for each flow rate for every experimental run to find the average velocity to increase the accuracy of this process. By finding the flow velocity, this result can translate into other findings such as finding the force subjected onto setae at a later stage.

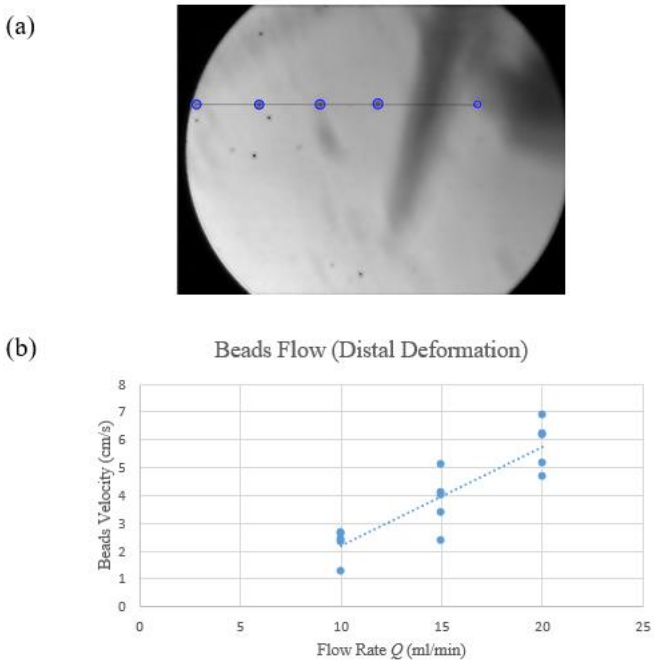

Figure 5-1 a) Superimposed image of microbeads flow in 5 frames captured by high speed camera b) Quantification of microbeads velocity from each flow rate

5.3 Capturing Setal Deformation

The focus of this experiment is to successfully capture the displacement of setae on the first antennae when subjected to a hydrodynamic disturbance. For each copepod specimen, the seta of interest is subjected to three flow rates from the set on the syringe pump at 10 mL/min, 15 mL/min and 20 mL/min to observe an effective range of deformation. Multiple runs are done with the defined flow rates to observe deformation of setae on different segments of the

first antenna. Figures 5-2 and 5-3 show each of the experimental runs for distal and proximal bending. Figure 5-2 shows the long type of seta being displaced from the seta's starting position to the final position. Similarly, the specimen is then placed on the opposite side of the flow outlet such that the flow is perpendicular to the seta to observe proximal bending (Figure 5-3), the three defined flow rates are executed for the proximal bending segment as well. When comparing deformation between distal and proximal direction, the seta displaces much lesser when bent towards the proximal direction. This shows a certain extent of bidirectional sensitivity when subjected to a disturbance which bends the seta towards the distal section.

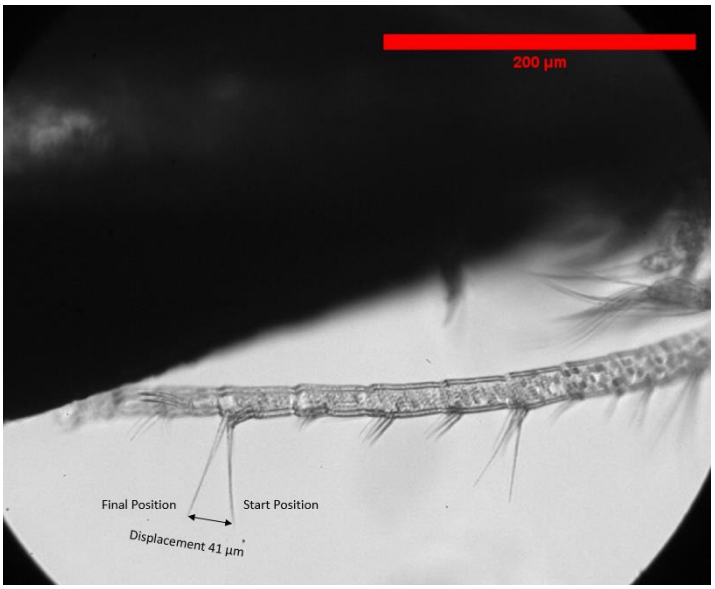

Figure 5-2 Deformation of long seta on first antenna when subjected to flow from syringe pump towards distal direction, showing initial and final positions of seta

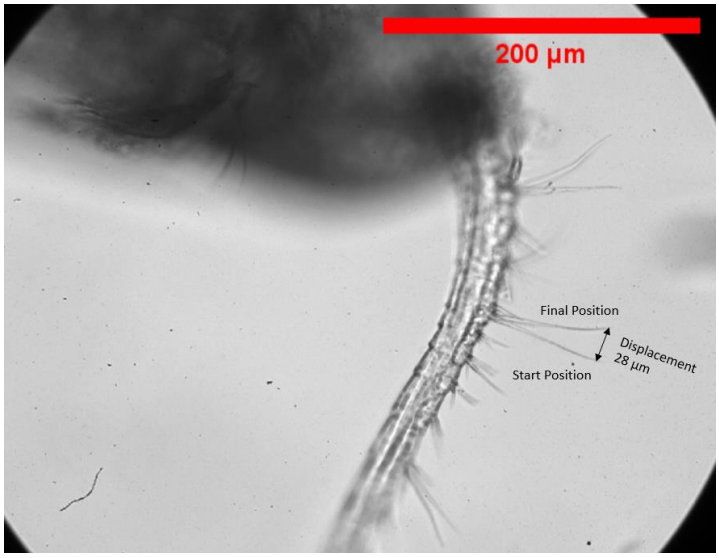

Figure 5-3 Deformation of long seta on first antennae towards proximal end when subjected to artificial stimulus by syringe pump, showing individual positions of displacement

5.3.1 Deformation Quantification

The three defined flow rates of this experimental study are chosen to observe an effective range of displacement on the smooth and long type of seta on the first antennae, as well as to compare the deformation as the flow rate increases for both distal and proximal bending (Figures 5-4 to 5-9).

Figure 5-4 Distal bending of long seta on the distal end, when subjected to flow of 10mL/min

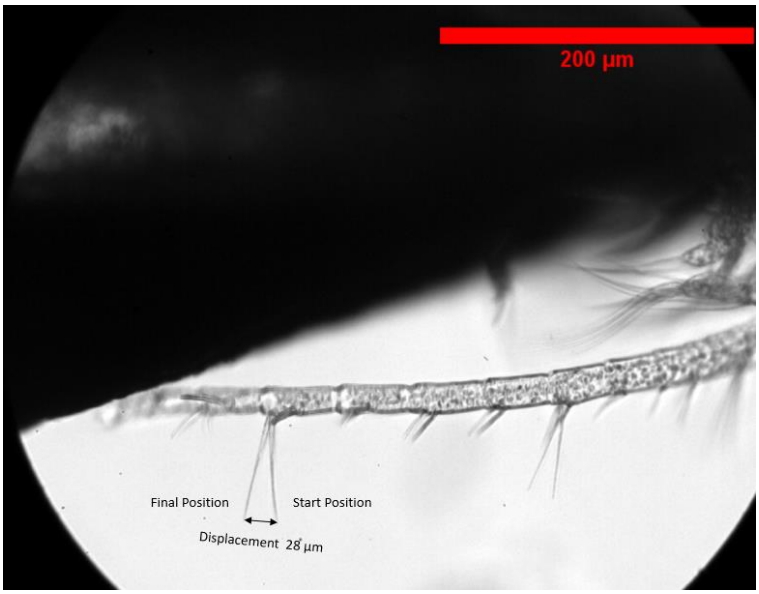

Figure 5-5 Distal bending of long seta on the distal end, when subjected to flow of 15mL/min

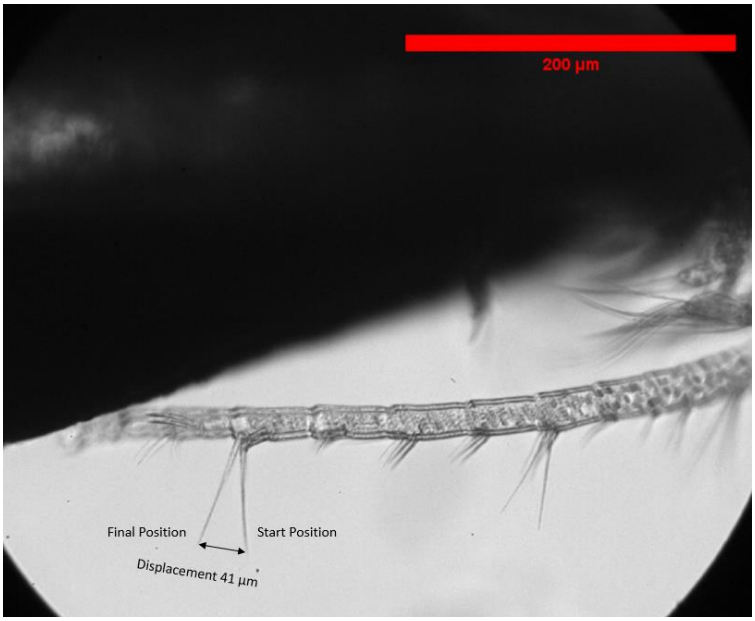

Figure 5-6 Distal bending of long seta on the distal end, when subjected to flow of 20mL/min

In one of the experimental runs, a long and smooth type of seta is observed and captured to compare the deformation when subjected to different flows. In Figure 5-4, is a superimposed image between the starting position of the observed seta and the final position, showing significant deformation of 15 µm in the distal direction when subjected to a flow of 10mL/min. When subjected to a higher flow rate of 15mL/min, the seta is displaced even more from its initial position, having a displacement of 28 µm towards the distal end (Figure 5-5). At the highest of the defined flow rate set out in this experiment, the deformation is found to be greatest at 41 µm towards the distal end when subjected to a flow of 20mL/min (Figure 5-6).

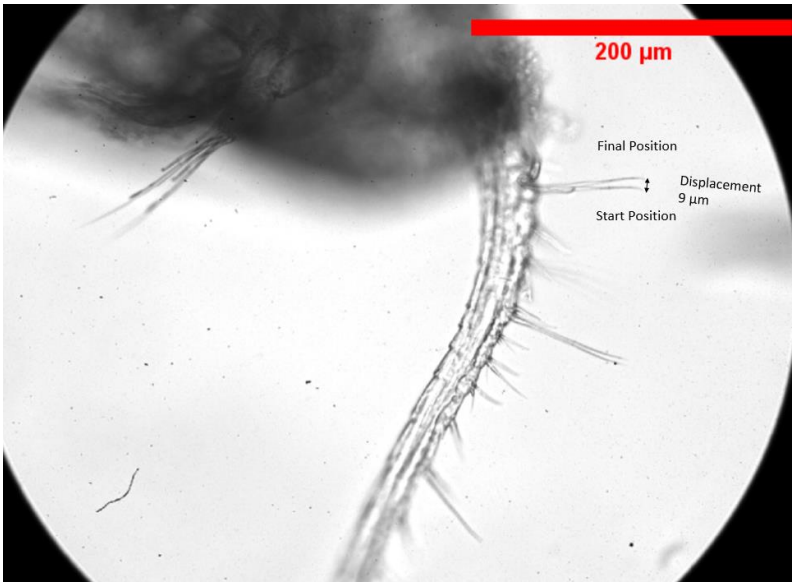

Figure 5-7 Proximal bending of long seta on the proximal end, subjected to flow of 10mL/min

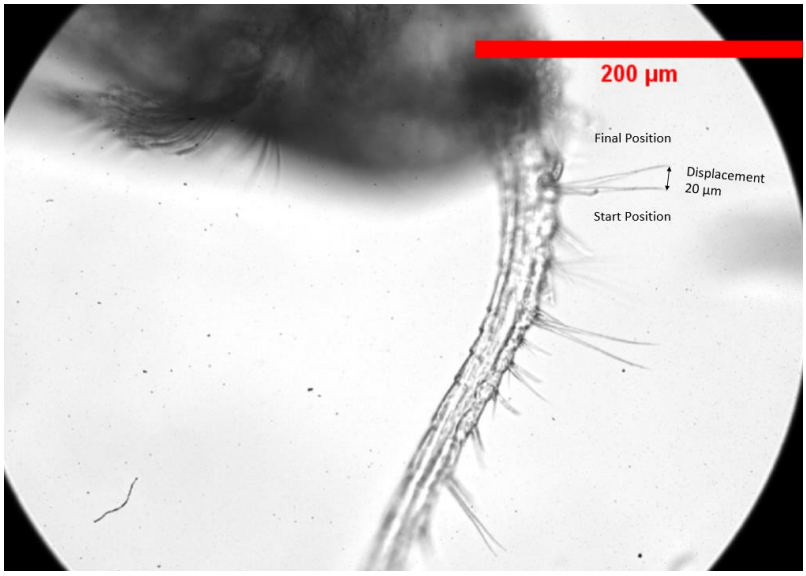

Figure 5-8 Proximal bending of long seta on the proximal end, subjected to flow of 15mL/min

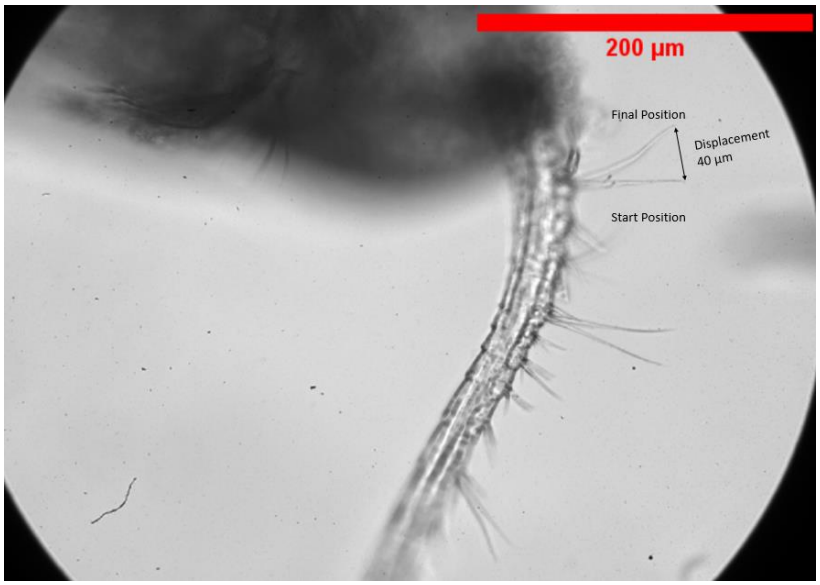

Figure 5-9 Proximal bending of long seta on the proximal end, subjected to flow of 20mL/min

Similarly, proximal bending is observed under the scope to compare the distal bending deformation of the smooth and long type of setae. Firstly, when subjected to a

flow of 10mL/min, minimum bending is observed as seen in Figure 5-7, with a displacement of 9μm. Secondly, when the seta is subjected to the next higher flow rate of 15mL/min, a greater displacement is observed of 20μm (Figure 5-8). Lastly, the greatest displacement towards the proximal end is observed at 40μm when subjected to a flow rate of 20mL/min (Figure 5-9).

5.3.2 Comparison of Deformation of Setae

The experimental runs focus specifically on the smooth and long type of seta on the first antennae, such that a fair comparison can be made from the different flow rates and between distal and proximal bending. For each flow rate in each experimental run, the exact velocity of the flow subjected on the seta is verified, making use of the microbeads method so the position changes of the specimen for every run will not affect the comparison of the deformation data. The deformation results are compared among setae from each segment of the first antenna. The results represented in the figures below belong to deformation data from Seta #1, Seta #3 and Seta #4, and they originate from the proximal, middle and distal segments respectively. Moreover, since both Seta #1 and #2 belong in the proximal segment, the deformation experiments focuses on Seta #1 for the proximal seta.

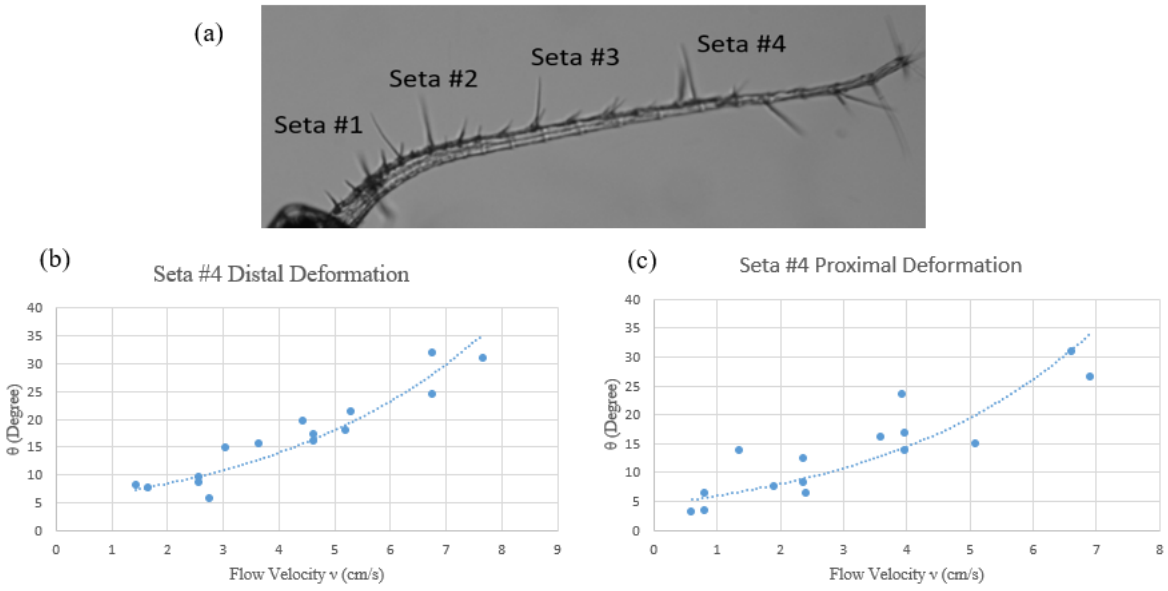

Figure 5-10 Flow Velocity (cm/s) vs Deformation (μm) for Distal Deformation of Distal Seta (Seta #4)

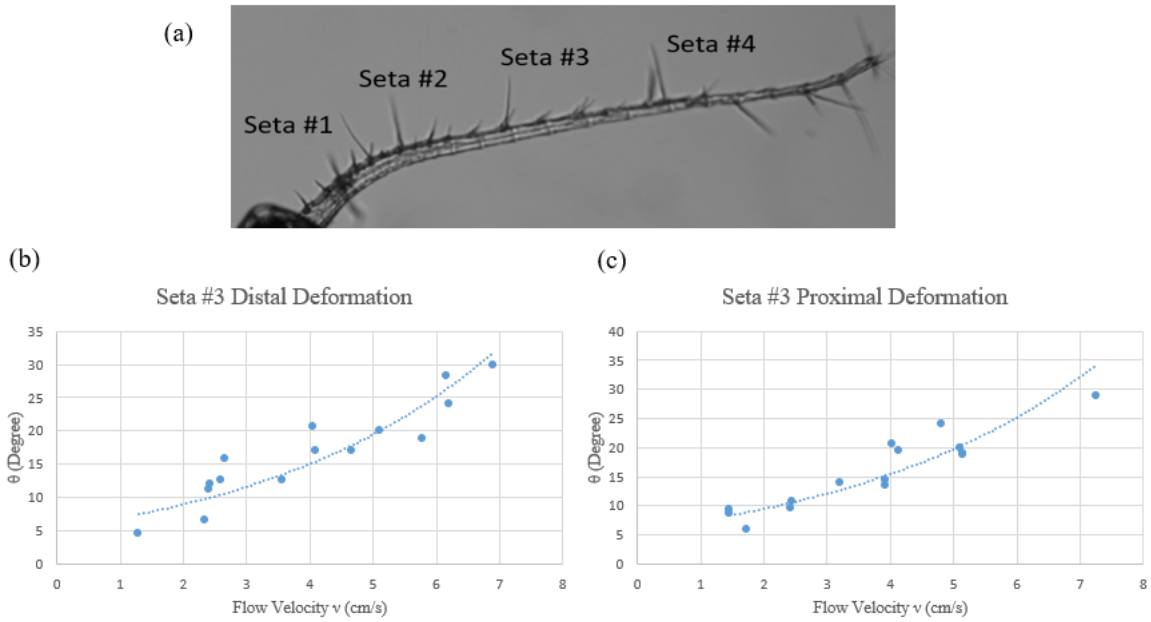

Figure 5-11 Flow Velocity (cm/s) vs Deformation (μm) for Distal Deformation of Middle Seta (Seta #3)

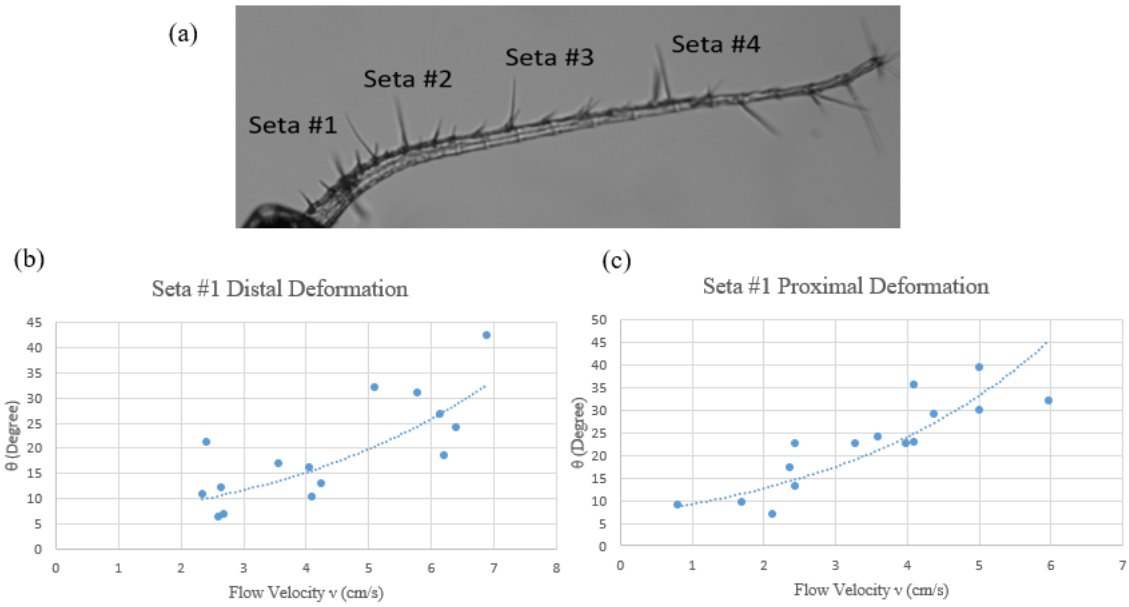

Figure 5-12 Flow Velocity (cm/s) vs Deformation (μm) for Distal Deformation of Proximal Seta (Seta #1)

Figures 5-10(b) to 5-12(b) reviews the deformation data for Seta #1, #3 and #4 when subjected to a flow to observe the distal deformation of these setae. These data are obtained from five experimental runs on each seta, belonging to five individual specimens that are shown in these plots. Although the flow rates are fixed for each experiment, the actual flow velocities subjected onto the setae are calculated and verified through the microbeads method for a more accurate comparison due to the variability of the specimen's position in the siphon device.

Firstly, to compare the distal deformations among the three setae, for the distal seta, which is Seta #4 in this study, the data shows rather close figures for the respective velocities with respect to distal deformation (Figure 5-10(b)). As the flow velocity increases, there is a trend showing an exponential increase in deformation from the seta's original upright position. The minimum deformation observed from Seta #4 is 7

degrees from its original position, and a maximum of 58 degrees. Figure 5-11(b) represents the distal deformation data plotted against the flow velocities of Seta #3. The data shows a similar exponential trend as compared to the data from Seta #4. However, the exponential increase in deformation with increase in velocity is more gradual in for Seta #3. The smallest deformation observed is 5 degrees and almost 30 degrees for the largest deformation in this case. In Figure 5-12(b), it shows the distal deformation data for Seta #1, which is the long and smooth type of seta that is closest to the proximal side of the first antenna. The data shows a wider range of variation of distal deformation observed from the experimental runs, with a similar gradual exponential trend. The minimum deformation at the lower velocities has larger variations, and it is similar at the higher end of deformation towards the distal direction. For the lower end, it is observed to vary from 6 degrees to 20 degrees, and it varies from 18 degrees to 42 degrees when subjected to higher flow velocities. The variation could be due to its biological variance of each seta belonging to individual specimen, and this will be further discussed in the next section.

Figures 5-10(c) to 5-12(c) represent the proximal deformation data against the flow velocities of Seta #1, #3 and #4. Figure 5-10(c) shows the proximal deformation data plotted against the flow velocity for Seta #4. The proximal deformation of the distal seta deforms more gradually as compared to its distal deformation (Figure 5-10(b)). The plot shows a wide range of proximal deformation from 4 degrees on the lower end and 31 degrees on the higher end. For Seta #3 in the middle segment of the antenna (Figure 5-11(c)), the results from the proximal deformation shows a more gradual exponential trend in terms of deformation against flow velocity, as compared to its distal deformation (Figure 5-10(b)), which is similar to Seta #4. Seta #3 shows a range of deformation across the velocities from 6 degrees to 29 degrees, having a slightly

smaller range as compared to Seta #4. For the proximal seta, Seta #1, Figure 5-12(c) shows a rather large range of deformation over the increasing flow velocities, from 7 degrees to 39 degrees, which also has the largest range of deformation among the three setae. Seta #1 has a wider range of proximal deformation as compared to its deformation towards the distal direction (Figure 5-12(b)).

6 Estimating Spring Constant

6.1 Seta Spring Model

This section explains the process of estimating the spring constant value by a simple model depicting deformation of seta as it is subjected to a force by the flow in the experimental runs as it is attached to its setal root. This is achieved by using the experimental results attained in this project, and adopting the resistive force theory to eventually estimate the spring constant for each type of seta. The Resistive Force Theory [58] is manipulated in this case assuming the flow is uniformed and the force is perpendicular, that is subjected onto the seta of interest,

$$F = C_{\perp} v \ L \tag{6-1}$$

where F is the force subjected on the subject seta, C is reported to be the normal drag coefficient, v is the velocity of the flow and L is the length of the subject seta.

Assuming a cylindrical seta with length L and radius R, the normal drag coefficient [59] is found to be,

$$C_{\perp} = 4\pi\mu[\ln\left(0.18\ \frac{L}{R}\right) + 0.5 \tag{6-2}$$

where μ is the viscosity of water, L is the length of the seta and R is the radius of the seta.

The moment M on seta caused by the flow force onto the seta is given by,

$$M = \int_0^L C_{\perp}\, v\ l\ dl \tag{6-3}$$

where $C_{\perp}$ is the normal drag coefficient, a specific flow velocity v, and l is the length of the subject seta.

Assuming a uniform flow, and a perpendicular force is subjected on the middle of the seta,

$$M = F\ \frac{L}{2} \tag{6-4}$$

where M is the moment caused by the force F on the halfway position of the seta's length.

The moment of seta subjected by the flow force is given by,

$$M = k\,\theta \tag{6-5}$$

where k is the spring constant of modelled spring of seta and θ is the angle of displacement

In (6-1), it depicts how the force subjected on seta is calculated. Thus, after calculating the drag coefficient value in equation (4-2), and with the data of the flow velocity and seta length, the force value is found using equation (4-1). Equation (4-4) is manipulated from equation (4-3), with the assumption that the flow subjected onto the seta is uniform. Thus, the moment caused by the force onto the seta is calculated using equation (4-4), also with the assumption the force is subjected on to middle of the seta (Figure 6-1(a)). Finally, with the displacement angle value in equation (4-5), the spring constant, k, is estimated using the experimental results of deformation in the previous chapter.

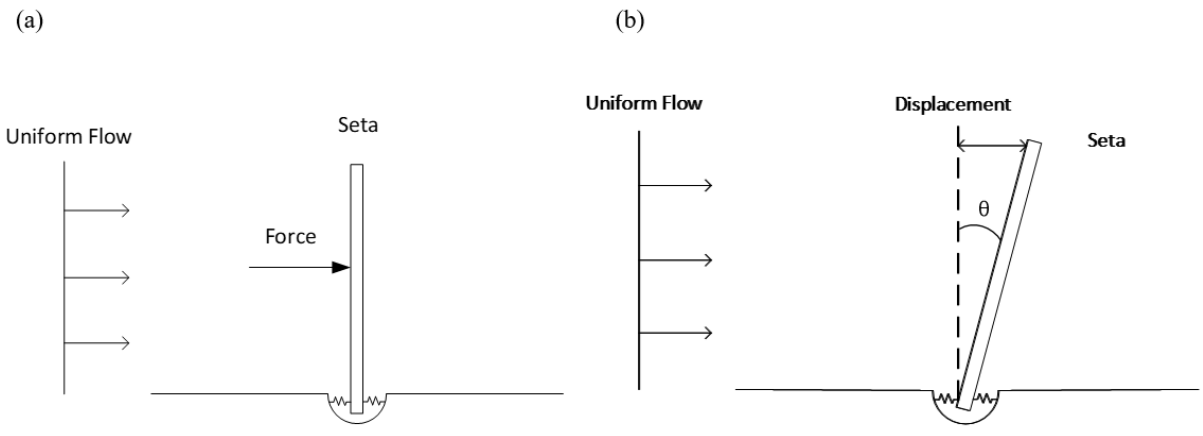

Figure 6-1 a) Left Image: Simple Spring Model representing seta and illustrating the force subjected onto seta by a uniform flow. b) Right Image: Seta displaced by the force from the uniform flow

The seta spring model in this study is based on the following assumptions. Firstly, a uniform flow is assumed to be subjected onto the seta using first order approximation of the flow velocity. The force from the flow is also assumed to be perpendicular to the seta and acting on the middle of the length of the subject seta. Next, the viscosity of the water is assumed to be constant throughout the experiment process, as there is no addition of other fluids into the petri dish. Low Reynolds number is assumed of the flow, and justified from the experimental data. Lastly, the force distribution is proportional to the local lateral velocity difference between the seta and the hydrodynamic flow as the subject specimen remains static.

The artificial stimulus in this study uses a siphon flow, which realistically is not uniformed at different radius points from the center of the syringe needle outlet. However, it is considered uniform across the length of the seta the flow is subjected on. Over the length of seta, the change in flow over the flow velocity is so small it is negligible, we take it as uniform flow over the length of seta.

$$u = \frac{Q}{2\pi r h} \tag{6-6}$$

where u represents flow velocity along the radius of flow from the center of the flow output the seta's position, Q is the flow rate depicted in the experiment and controlled by the syringe pump and r represents the distance from the center of the output flow to the position of subject seta, h is the height of the water present in the petri dish.

$$\Delta u = \frac{Q}{2\pi r h} - \frac{Q}{2\pi (r+L) h} \tag{6-7}$$

$$= -\frac{Q}{2\pi r^2 h} L$$

Δu represents the change in flow velocity along the length of subject seta, L is the length of the subject seta

$$\frac{\Delta u}{u} = \frac{-\frac{Q}{2\pi r^2 h} L}{\frac{Q}{2\pi r h}} \tag{6-8}$$

$$= -\frac{L}{r}$$

$\frac{\Delta u}{u}$ represents the fraction of change in flow velocity compared to the original flow velocity

The equations above, 4-6 to 4-8 verifies the assumption of a uniform flow the subject seta is subjected to. Equation 4-6 depicts the flow velocity in relation to the distance from the center of the flow outlet, and equation 4-7 shows the change in flow velocity in relation to the length of seta. Thus, in equation 4-8 shows that the change in flow velocity as compared to the original flow velocity is negligible, so a uniform flow is assumed in this case.

6.2 Discussion on Estimated Spring Constants

A simple seta-spring model (Figure 6-1) is used to illustrate the deformation of setae as a spring model at the setal root, to estimate the spring constant values of Seta #1, #3 and #4, utilizing the experimental data and the above methods. In Figure 6-1(a), the force subjected onto seta by the uniform flow, is assumed to be at the halfway point of the length of the seta. Figure 6-1(b) shows the final position after it has been displaced by a certain flow, depicting the resistance at the root with a spring concept to estimate this spring constant as most of the deformation happens at the root.

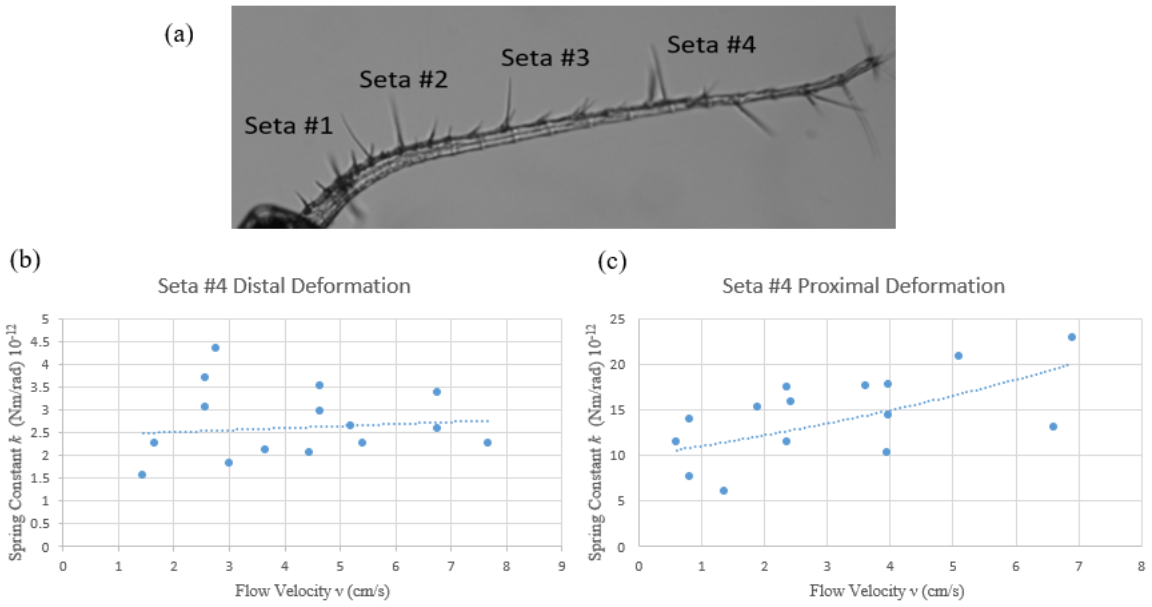

Figure 6-2 Spring Constant vs Flow Velocity for Seta #4 from both Proximal and Distal Deformation

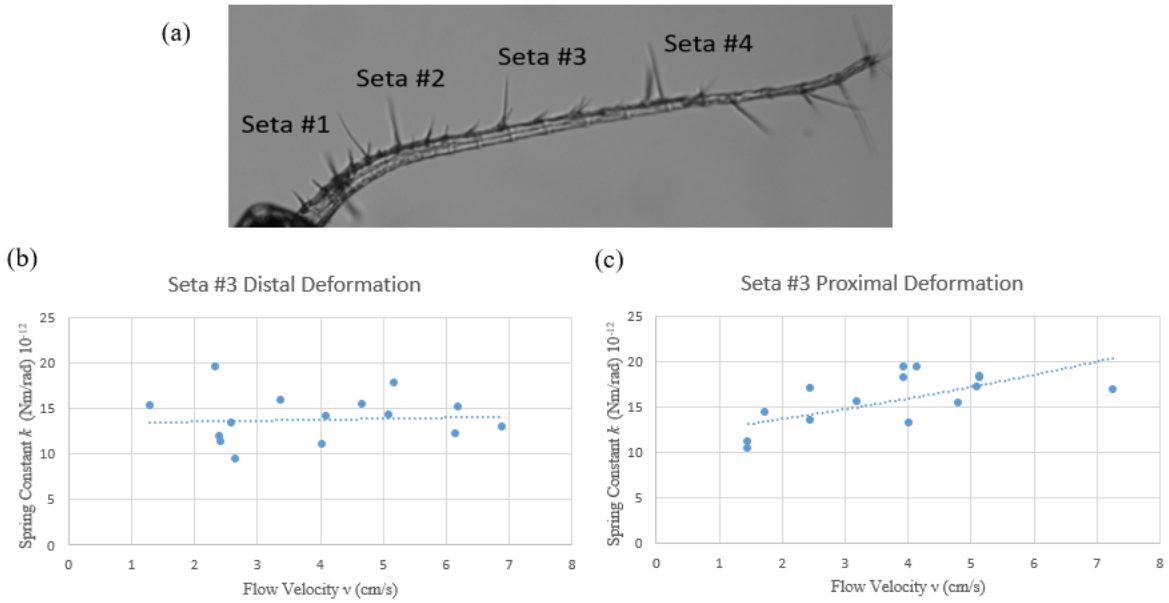

Figure 6-3 Spring Constant vs Flow Velocity for Seta #3 from both Proximal and Distal Deformation

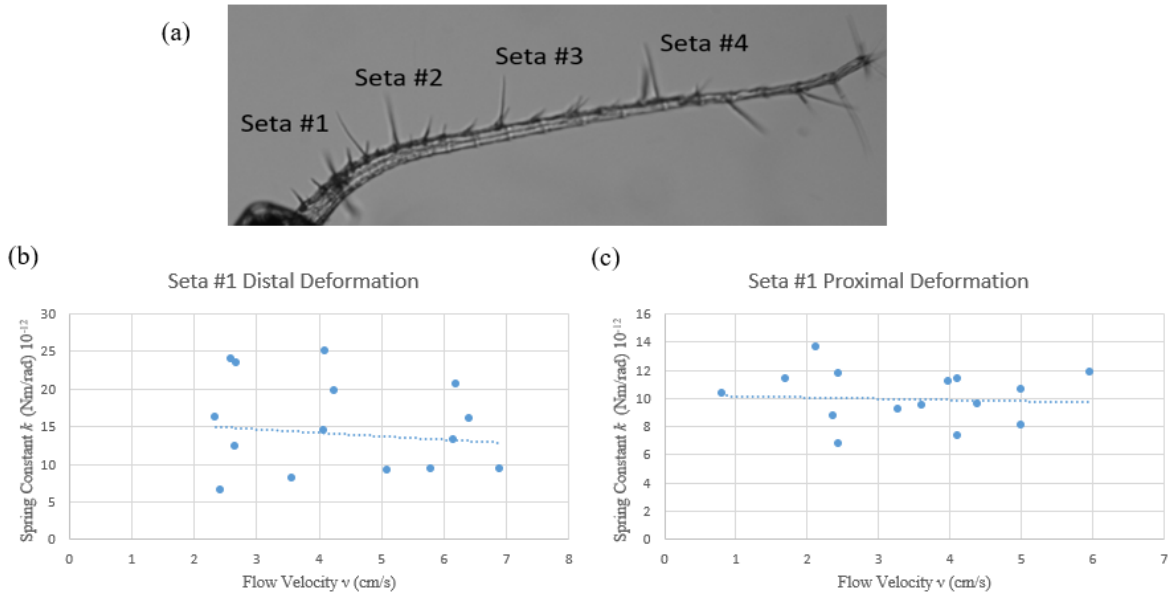

Figure 6-4 Spring Constant vs Flow Velocity for Seta #1 from both Proximal and Distal Deformation

In the above Figures 6-2 to 6-4, plots the data of the estimated spring constants attained through experimental and morphological results. Using the concept of Resistive Force Theory and Equations 4-1 to 4-4, the spring constant values are estimated using the deformation and setae data for each seta in different segments of the first antenna. The experimental runs were carried out on five specimens for each of the three segments on the first antenna, for both proximal and distal deformation. The purpose of these plots are to compare the spring constant values for each seta among different specimens.

In Figure 6-2, it shows the estimated spring constant values of Seta #4 as the flow velocity increases for both proximal and distal deformation. There is a significant difference in range between the spring constants estimated in the distal deformation and proximal deformation phase. From the distal deformation results (Figure 6-2(b)), the spring constants are much lower which have values below 5×10^{-6} Nm/rad. On the other hand, the spring constants obtained from the proximal deformation results (Figure 6-2(c)) are significant higher, ranging from 6 to 23×10^{-6} Nm/rad. This shows there is a certain extent of directional sensitivity or biasness for Seta #4 in this case as the seta is less stiff when deformed towards the distal direction.

The estimated spring constants for Seta #3 are shown in Figure 6-3. For Seta #3, the spring constants obtained from both proximal (Figure 6-3(c)) and distal deformation (Figure 6-3(b)) results do not differ significantly and are found to be within the range of 9.5 to 19×10^{-6} Nm/rad. However, there are slightly different trends among the middle setae. A gradual linear increment is observed when Seta #3 is formed proximally as the flow velocity increases. Generally, Seta #3 is observed to have a higher spring constant than Seta #4.

Lastly, the estimated spring constants for the proximal seta, Seta #1 are seen in Figure 6-4. Most of the spring constants obtained are seen to be within the same range between 5 to 15 $\times 10^{-6}$ Nm/rad, which has the similar range value but lower in this case as compared to Seta #3.

Most of these setae are observed to have constant or gradual change in the spring constant value as the flow velocity increases. The estimated spring constants from the distal deformation data shows a very gradual linear decrease as the flow velocity increases. On the other hand, the spring constant from the proximal deformation results are observed to be a rather constant throughout. Seta #1 has lower spring constants as compared to Seta #3 for most of the setae, which means Seta #1 is less stiff and deforms more easily than Seta #3 when subjected to the same flow force. Seta #4 has the lowest spring constant when deformed towards the distal direction, which means it deforms easily distally which may give rise to a stronger neuro signal which affects the outcome of the copepod's behaviour, and on the other hand, Seta #3 is the stiffest when deformed towards the proximal direction.

7 Conclusion & Future Work

7.1 Conclusion

In the preliminary observations, the external morphology was established to be similar to past studies and also showed that setal deformation on the first antennae can be achieved with artificial stimulus with the current experimental set up. Through the experimental runs, it is observed that the smooth and long type of seta has a certain extent of bidirectional sensitivity [60], with higher stiffness towards the proximal direction to a certain limit. Seta #4, in the distal segment, has the lowest spring constant when deformed towards the distal direction, thus, this property helps in sensitivity to a certain extent when subjected to hydrodynamic disturbance towards the distal end. Seta #3, in the middle segment, showed the most consistent spring constant results, with most setae being in the same range of spring constants for both proximal and distal deformations, and observed to be generally stiffer than Seta #4. For Seta #1, in the proximal region, most of the proximal setae has shown that it

deforms more easily towards the proximal side as compared to the distal direction. Thus, Seta #1 is considered to be less stiff than Seta #3 for proximal deformation. The differences between the three setae investigated in this study in terms of estimation of its spring constant values, suggest that individual seta has its own function and sensitivity, to be able to decipher the hydrodynamic disturbances from its source in terms of distance and direction from the copepod itself.

Nonetheless, the current work showed that with the presence of hydrodynamic disturbance, the displacement of setae can be analysed accurately with this experimental device and set up. These results can be considered in the future for further research to study its mechanical properties with appropriate numerical models.

7.2 Future Work

At this stage of the study, with the assumptions of the induced hydrodynamic flow and the properties of setae, it can only be concluded that the spring constant of seta increases with increasing flow velocity. Further studies will have to be done to find out if the spring constant varies differently under different parameters. Additionally, using the spring constant results obtained in this study, another future study can focus on whether the proximity between setae affects the spring constant, which can be an estimation of its abilities in relation to the proximity.

References

1. Tautz, J., *Reception of particle oscillation in a medium — an unorthodox sensory capacity.* Naturwissenschaften, 1979. **66**(9): p. 452-461.
2. Kjellerup, S. and T. Kiørboe, *Prey detection in a cruising copepod.* Biology Letters, 2012. **8**(3): p. 438-441.
3. Koehl, M.A.R. and J.R. Strickier, *Copepod feeding currents: Food capture at low Reynolds number1.* Limnology and Oceanography, 1981. **26**(6): p. 1062-1073.
4. Błędzki, L. and J. Rybak, *Freshwater Crustacean Zooplankton of Europe: Cladocera & Copepoda (Calanoida, Cyclopoida) Key to species identification, with notes on ecology, distribution, methods and introduction to data analysis*. 2016.
5. Santer, B., *Life cycle strategies of free-living copepods in fresh waters.* Journal of Marine Systems, 1998. **15**(1): p. 327-336.
6. Devarakonda, R., F.G. Barth, and J.A.C. Humphrey, *Dynamics of arthropod filiform hairs. IV. Hair motion in air and water.* Philosophical Transactions of the Royal Society of London. Series B: Biological Sciences, 1996. **351**(1342): p. 933-946.
7. Fields, D.M., D.S. Shaeffer, and M.J. Weissburg, *Mechanical and neural responses from the mechanosensory hairs on the antennule of Gaussia princeps.* Marine Ecology Progress Series, 2002. **227**: p. 173-186.
8. Bagøien, E. and T. Kiørboe, *Blind dating - Mate finding in planktonic copepods. I. Tracking the pheromone trail of Centropages typicus.* Marine Ecology-progress Series - MAR ECOL-PROGR SER, 2005. **300**: p. 105-115.
9. Borazjani, I., et al., *On the role of copepod antennae in the production of hydrodynamic force during hopping.* Journal of Experimental Biology, 2010. **213**(17): p. 3019-3035.
10. Weatherby, T. and P. Lenz, *Mechanoreceptors in calanoid copepods: Designed for high sensitivity.* Arthropod structure & development, 2000. **29**: p. 275-88.
11. Humphrey, J.A.C., F.G. Barth, and K. Voss. *The Motion-Sensing Hairs of Arthropods: Using Physics to Understand Sensory Ecology and Adaptive Evolution*. 2001. Berlin, Heidelberg: Springer Berlin Heidelberg.
12. Fields, D., *Fields, D.M. 2014. The sensory horizon of marine copepods, pp: 157-179, In, Seuront, L. (Ed.), Copepods: Diversity, Habitat and Behavior. Nova Science Publishers, Inc*. 2014. p. 157-179.
13. Humphrey, J.A.C. and F.G. Barth, *Medium Flow-Sensing Hairs: Biomechanics and Models*, in *Advances in Insect Physiology*, J. Casas and S.J. Simpson, Editors. 2007, Academic Press. p. 1-80.
14. Jiang, H. and G.A. Paffenhöfer, *Hydrodynamic signal perception by the copepod Oithona plumifera.* Marine Ecology Progress Series, 2008. **373**: p. 37-52.
15. Boxshall, G.A., et al., *Reading the copepod personal ads: increasing encounter probability with hydromechanical signals.* Philosophical Transactions of the Royal Society of London. Series B: Biological Sciences, 1998. **353**(1369): p. 691-700.
16. Kiørboe, T., *Sex, sex-ratios, and the dynamics of pelagic copepod populations.* Oecologia, 2006. **148**(1): p. 40-50.
17. Kiørboe, T., et al., *Mechanisms and feasibility of prey capture in ambush-feeding zooplankton.* Proceedings of the National Academy of Sciences, 2009. **106**(30): p. 12394.
18. Buskey, E.J., et al., *Escapes in copepods: comparison between myelinate and amyelinate species.* The Journal of Experimental Biology, 2017. **220**(5): p. 754.
19. Yen, J., et al., *Mechanoreception in marine copepods: Electrophysiological studies on the first antennae.* Journal of Plankton Research, 1992. **14**.

20. Weatherby, T.M., K.K. Wong, and P.H. Lenz, *Fine Structure of the Distal Sensory Setae on the First Antennae of Pleuromamma Xiphias Giesbrecht (Copepoda).* Journal of Crustacean Biology, 1994. **14**(4): p. 670-685.
21. Fleminger, A., *Dimorphism and possible sex change in copepods of the family Calanidae.* Marine Biology, 1985. **88**(3): p. 273-294.
22. Gill, C.W. and S.A. Poulet, *Utilization of a computerized micro-impedance system for studying the activity of copepod appendages.* Journal of Experimental Marine Biology and Ecology, 1986. **101**(1): p. 193-198.
23. Fields, D.M., D.S. Shaeffer, and M.J. Weissburg, *Mechanical and neural responses from the mechanosensory hairs on the antennule of Gaussia princeps.* Marine Ecology Progress Series, 2002. **227**: p. 173-186.
24. Yen, J. and N.T. Nicoll, *Setal Array on the First Antennae of a Carnivorous Marine Copepod, Euchaeta Norvegica.* Journal of Crustacean Biology, 1990. **10**(2): p. 218-224.
25. Lenz, P.H. and J. Yen. *Distal Setal Mechanoreceptors of the First Antennae of Marine Copepods*. 1993.
26. Strickler, J.R. and A.K. Bal, *Setae of the First Antennae of the Copepod Cyclops scutifer (Sars): Their Structure and Importance[*].* Proceedings of the National Academy of Sciences, 1973. **70**(9): p. 2656-2659.
27. Lenz, P.H. and D.K. Hartline. *MECHANORECEPTION IN CRUSTACEANS OF THE PELAGIC REALM*. 2015.
28. Strickler, J.R. and A. Bal, *Strickler JR, Bal AK.. Setae of the first antennae of the copepod Cyclops scutifer (Sars): their structure and importance. Proc Natl Acad Sci USA 70: 2656-2659.* Proceedings of the National Academy of Sciences of the United States of America, 1973. **70**: p. 2656-9.
29. Hartline, D.K., P.H. Lenz, and C.M. Herren, *Physiological and behavioral studies of escape responses in calanoid copepods.* Marine and Freshwater Behaviour and Physiology, 1996. **27**(2-3): p. 199-212.
30. Lenz, P.H. and D.K. Hartline, *Reaction times and force production during escape behavior of a calanoid copepod, Undinula vulgaris.* Marine Biology, 1999. **133**(2): p. 249-258.
31. Gill, C.W., *Recording the beat patterns of the second antennae of calanoid copepods, with a micro-impedance technique.* Hydrobiologia, 1987. **148**(1): p. 73-78.
32. Yen, J. and J.R. Strickler, *Advertisement and Concealment in the Plankton: What Makes a Copepod Hydrodynamically Conspicuous?* Invertebrate Biology, 1996. **115**(3): p. 191-205.
33. Garcia-Anoveros, J. and D.P. Corey, *The molecules of mechanosensation.* Annu Rev Neurosci, 1997. **20**: p. 567-94.
34. Haury, L.R., D.E. Kenyon, and J.R. Brooks, *Experimental evaluation of the avoidance reaction of Calanus finmarchicus1*. Journal of Plankton Research, 1980. **2**(3): p. 187-202.
35. Kiørboe, T., E. Saiz, and A. Visser, *Hydrodynamic signal perception in the copepod Acartia tonsa.* Marine Ecology Progress Series, 1999. **179**: p. 97-111.
36. Hudspeth, A.J. and P.G. Gillespie, *Pulling springs to tune transduction: Adaptation by hair cells.* Neuron, 1994. **12**(1): p. 1-9.
37. Shen, X., Marcos, and H.C. Fu, *How the bending mechanics of setae modulate hydrodynamic sensing in copepods.* Limnology and Oceanography, 2020. **65**(4): p. 749-761.
38. Laverack, M.S., D.L. Macmillan, and D.M. Neil, *A comparison of beating parameters in larval and post-larval locomotor systems of the lobster Homarus gammarus (L.).* Philos Trans R Soc Lond B Biol Sci, 1976. **274**(929): p. 87-99.
39. Ball, E.E., A.N. Cowan, and G.A. Horridge, *Ultrastructure of the antennal sensilla of Acetes (Crustacea, Decapoda, Natantia, Sergestidae).* Philosophical Transactions of the Royal Society of London. B, Biological Sciences, 1977. **277**(957): p. 429-456.

40. Weissburg, M.J., M.H. Doall, and J. Yen, *Following the Invisible Trail: Kinematic Analysis of Mate-Tracking in the Copepod Temora Longicornis.* Philosophical Transactions: Biological Sciences, 1998. **353**(1369): p. 701-712.
41. Fields, D., D. Shaeffer, and M. Weissburg, *Mechanical and neural responses from the mechanosensory hairs on the antennule of Gaussia princeps.* Marine Ecology Progress Series, 2002. **227**: p. 173-186.
42. Markku, V., et al., *Predation vulnerability of planktonic copepods: consequences of predator foraging strategies and prey sensory abilities.* Marine Ecology Progress Series, 1998. **175**: p. 129-142.
43. Kiørboe, T., *How zooplankton feed: mechanisms, traits and trade-offs.* Biological Reviews, 2011. **86**(2): p. 311-339.
44. van Duren, L.A. and J.J. Videler, *Escape from viscosity: the kinematics and hydrodynamics of copepod foraging and escape swimming.* Journal of Experimental Biology, 2003. **206**(2): p. 269.
45. Lenz, P. and J. Yen. *Distal Setal Mechanoreceptors of the First Antennae of Marine Copepods*. 1993.
46. Strickler, J.R., *Swimming of planktonic Cyclops species (Copepoda, Crustacea): pattern, movements and their control*, in *Swimming and flying in nature*. 1975, Springer. p. 599-613.
47. Waggett, R.J. and E.J. Buskey, *Escape reaction performance of myelinated and non-myelinated calanoid copepods.* Journal of Experimental Marine Biology and Ecology, 2008. **361**(2): p. 111-118.
48. Yen, J. and A. Okubo, *Particle and prey detection by mechanoreceptive copepods: a mathematical analysis.* Hydrobiologia, 2002. **480**(1): p. 165-173.
49. Alcaraz, M., A. G, and J.R. Strickler, *Catching the algae: A first account of visual observations on filter-feeding calanoids.* Evolution and Ecology of Zooplankton Communities, 1980: p. 241-248.
50. Gans, C., *Biomechanics: Mechanical Design in Organisms. S. A. Wainwright, W. D. Biggs, J. D. Currey, and J. M. Gosline. Halsted (Wiley), New York, 1976. xii, 424 pp., illus. $19.50.* Science, 1976. **194**(4268): p. 933-934.
51. Gassie, D.V., et al., *Mechanoreception in zooplankton first antennae: electrophysiological techniques.* Bulletin of Marine Science, 1993. **53**(1): p. 96-105.
52. Houshuo, J. and P.Â.f. Gustav-Adolf, *Relation of behavior of copepod juveniles to potential predation by omnivorous copepods: an empirical-modeling study.* Marine Ecology Progress Series, 2004. **278**: p. 225-239.
53. Deurs, M., A. Christensen, and A. Rindorf, *Patchy zooplankton grazing and high energy conversion efficiency: Ecological implications of sandeel behavior and strategy.* Marine Ecology Progress Series, 2013. **487**: p. 123-133.
54. Kiørboe, T. and H. Jiang, *To eat and not be eaten: optimal foraging behaviour in suspension feeding copepods.* Journal of The Royal Society Interface, 2013. **10**(78): p. 20120693.
55. Bundy, M.H., et al., *Perception of inert particles by calanoid copepods: behavioral observations and a numerical model.* Journal of Plankton Research, 1998. **20**(11): p. 2129-2152.
56. Kiørboe, T., *A Mechanistic Approach to Plankton Ecology.* ASLO Web Lectures, 2009. **1**(2): p. 1-91.
57. K S, S. and S. Bijoy Nandan, *Morphological discrimination of female specimens of Pseudodiaptomus annandalei from Cochin estuary and Corbyn's Cove Creek, India.* Indian Journal of Geo-Marine Sciences, 2019. **48**: p. 302-308.
58. Gray, J. and G.J. Hancock, *The Propulsion of Sea-Urchin Spermatozoa.* The Journal of Experimental Biology, 1955. **32**: p. 802-814.
59. Lighthill, J., *Flagellar Hydrodynamics: The John von Neumann Lecture, 1975.* SIAM Review, 1976. **18**(2): p. 161-230.

60. Takagi, D. and D.K. Hartline, *Directional Hydrodynamic Sensing by Free-Swimming Organisms.* Bulletin of Mathematical Biology, 2018. **80**(1): p. 215-227.